Elastic response of the electron fluid in intrinsic graphene: The collisionless regime

Julia M. Link, Daniel E. Sheehy, Boris N. Narozhny, and Jörg Schmalian

Phys. Rev. B **98**, 195103 — Published 2 November 2018

DOI: 10.1103/PhysRevB.98.195103

Elastic response of the electron fluid in intrinsic graphene: the collisionless regime

Julia M. Link,[1] Daniel E. Sheehy,[2] Boris N. Narozhny,[1,3] and Jörg Schmalian[1,4]

[1] *Institute for Theory of Condensed Matter, Karlsruhe Institute of Technology (KIT), 76131 Karlsruhe, Germany*
[2] *Department of Physics and Astronomy, Louisiana State University, Baton Rouge, LA, 70803, USA*
[3] *National Research Nuclear University MEPhI (Moscow Engineering Physics Institute), 115409 Moscow, Russia*
[4] *Institute for Solid State Physics, Karlsruhe Institute of Technology (KIT), 76131 Karlsruhe, Germany*

(Dated: October 9, 2018)

The elastic response of an electron fluid at finite frequencies is defined by the electron viscosity $\eta(\omega)$. We determine $\eta(\omega)$ for graphene at the charge neutrality point in the collisionless regime, including the leading corrections due to the electron-electron Coulomb interaction. We find interaction corrections to $\eta(\omega)$ that are significantly larger if compared to the corresponding corrections to the optical conductivity. In addition, we find comparable contributions to the dynamic momentum flux due to single-particle and many-particle effects. We also demonstrate that $\eta(\omega)$ is directly related to the nonlocal energy-flow response of graphene at the Dirac point. The viscosity in the collisionless regime is determined with the help of the strain generators in the Kubo formalism. Here, the pseudo-spin of graphene describing its two sublattices plays an important role in obtaining a viscosity tensor that fulfills the symmetry properties of a rotationally symmetric system.

I. INTRODUCTION

The low-frequency flow of electron charge and momentum in graphene is dissipative[1–3] and can be described within the hydrodynamic approach[4–7]. Signatures of hydrodynamic behavior in graphene have been recently observed experimentally[8–12] while attracting considerable theoretical attention[13–17].

The collective motion of charge carriers in a solid becomes hydrodynamic, if the dominant scattering mechanism is provided by electron-electron interactions, such that the corresponding scattering rate τ_{ee}^{-1} multiplied by Planck's constant, $\hbar\tau_{ee}^{-1}$, is the largest energy scale in the problem[6,7]. For example, the low-frequency, $\omega\tau_{ee} < 1$, Drude-type dynamical viscosity due to collisions of thermally excited carriers is shown in the inset of Fig. 1. Stationary transport properties are then encoded in a few kinetic coefficients describing dissipative processes[18]. In contrast to standard fluid mechanics[4,18], dissipation in graphene is described by the electrical (rather than the thermal) conductivity at the charge neutrality point and the shear and bulk viscosities[6]. The former reflects the particular property of Dirac fermions in graphene in which the energy current is proportional to the total momentum and is conserved by electron-electron interactions. The electric current is not conserved and at charge neutrality can be relaxed by electron-electron interactions[19,20]. The bulk viscosity in graphene was argued to vanish[3,7,13], at least within the considered approximations.

At relatively high frequencies, i.e. in the optical collisionless regime, $\omega\tau_{ee} \gg 1$, free Dirac fermions in pure graphene at charge neutrality are characterized by the frequency-independent optical conductivity[21–32], while electron-electron interactions yield a rather small, weakly frequency-dependent correction:

$$\sigma(\omega) = \frac{\pi e^2}{2h}\left[1 + \mathcal{C}_\sigma \alpha(\omega)\dots\right], \quad \alpha(\omega) = \frac{\alpha_0}{1+\frac{\alpha_0}{4}\ln\frac{D}{\omega}}. \quad (1)$$

Here $\alpha(\omega)$ is a running (or renormalized) dimensionless coupling constant measuring the strength of the Coulomb interaction, $\alpha_0 = e^2/(\hbar v\bar{\epsilon})$ is its bare value, e is the electron charge, v is the bare velocity of the Dirac fermions, D is the bandwidth scale, and $\bar{\epsilon} = (\epsilon_1+\epsilon_2)/2$ is determined by the dielectric constants $\epsilon_{1,2}$ of the material above and below the graphene sheet (in suspended graphene $\bar{\epsilon} = 1$ and $\alpha_0 \approx 2.2$). Our results are obtaind using a perturbative renormalization group analysis. While α_0 is of order unity, the expansion is in fact with regards to the renormalized coupling constant $\alpha(\omega)$ of Eq. 1 which is small for $\omega \ll D$. The numerical coefficient $\mathcal{C}_\sigma = (19-6\pi)/12 \approx 0.01$ is rather small[23,24,31,32]. This is in agreement with the experimental measurement[33] of the transmission coefficient related to the conductivity by[34] $T(\omega) = [1+2\pi\sigma(\omega)/c]^{-2}$: the measured value $T = 0.977$ yields $\sigma(\omega) \approx \pi e^2/(2h)$.

In this paper we consider the electronic viscosity of graphene in the collisionless regime, with a particular emphasis on understanding the impact of electron-electron interactions on this observable. We start by noting that the behavior of the electronic fluid in graphene at finite frequencies is similar to that of an elastic medium[35]. Elastic deformations are described in terms of a dynamic strain

$$\varepsilon_{\gamma\delta}(\boldsymbol{x},t) = \frac{\partial u_\delta(\boldsymbol{x},t)}{\partial x_\gamma}, \quad (2)$$

where the vector $\boldsymbol{u}(\boldsymbol{x},t)$ describes the displacement of a fluid element. Within the elasticity theory, the strain is linearly related to stress. If $\langle\tau_{\alpha\beta}(\boldsymbol{x})\rangle$ is the expectation value of the stress tensor operator and $\delta\langle\tau_{\alpha\beta}\rangle$ is the change in $\langle\tau_{\alpha\beta}\rangle$ from its value for zero strain, $\varepsilon_{\gamma\delta} = 0$, then we can define the dynamic elastic response constants by

$$\delta\langle\tau_{\alpha\beta}\rangle(t) = \int_{-\infty}^{\infty} dt' C_{\alpha\beta\gamma\delta}(t-t')\varepsilon_{\gamma\delta}(t'). \quad (3)$$

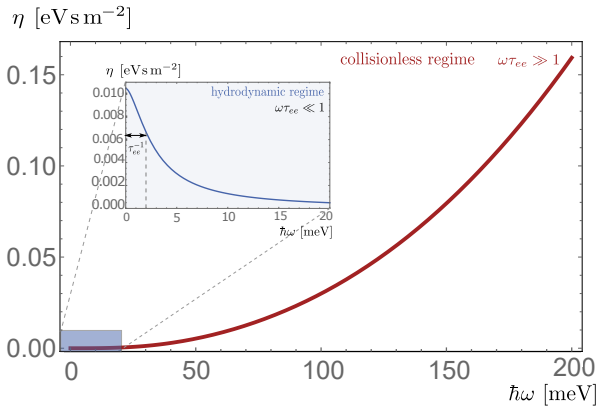

FIG. 1. (Color Online) Main: Frequency-dependent shear viscosity, Eq.(6), in pure graphene at charge neutrality and temperature $T = 0$ in the high-frequency collisionless regime. Inset: Frequency-dependent shear viscosity in the low-frequency hydrodynamic regime for $T = 100$ K and an inverse scattering time of $\hbar\tau_{ee}^{-1} \simeq 1.307\ \alpha_0^2 k_B T \simeq 0.002$ eV obtained by generalizing the analysis of Ref. 3 to small but finite frequencies[36].

In the collisionless regime, the dynamic elastic constants can be split into isothermal and adsorptive parts (see section II for a formal proof) with the latter related to the dynamic viscosity, $\eta_{\alpha\beta\gamma\delta}(\omega)$:

$$C_{\alpha\beta\gamma\delta}(\omega) = C^T_{\alpha\beta\gamma\delta} - i\omega\eta_{\alpha\beta\gamma\delta}(\omega), \tag{4}$$

In an isotropic fluid, the elastic properties are determined by the bulk modulus, hence the isothermal static elastic constant is equal to

$$C^T_{\alpha\beta\gamma\delta} = \kappa_T^{-1}\delta_{\alpha\beta}\delta_{\gamma\delta}, \qquad \kappa_T^{-1} = -V\left.\frac{\partial p}{\partial V}\right|_{N,T},$$

with κ_T the isothermal compressibility.

In systems with rotational invariance (which holds for graphene in the low-energy limit), the tensor structure of the dynamic viscosity has the form[4]

$$\eta_{\alpha\beta\gamma\delta}(\omega) = \eta(\omega)\left[\delta_{\alpha\gamma}\delta_{\beta\delta} + \delta_{\alpha\delta}\delta_{\beta\gamma} - \frac{2}{d}\delta_{\alpha\beta}\delta_{\gamma\delta}\right], \tag{5}$$

where $\eta(\omega)$ is the shear viscosity, d is the dimensionality, and we neglected the bulk viscosity[3,7,13].

Our main result concerns $\eta(\omega)$ in the the collisionless regime of pure graphene at the charge neutrality point (and at zero temperature, $T = 0$). We obtain

$$\eta(\omega) = \frac{\hbar}{64}\frac{\omega^2}{v^2(\omega)}\left[1 + \mathcal{C}_\eta\alpha(\omega) + \mathcal{O}[\alpha^2(\omega)]\right], \tag{6}$$

with the numerical coefficient

$$\mathcal{C}_\eta = \frac{89 - 20\pi}{40} \approx 0.65 \gg C_\sigma.$$

Here, $v(\omega) = v[1 + (\alpha_0/4)\ln(D/\omega)]$ is the renormalized velocity at frequency ω. The resulting frequency dependence of the viscosity is shown in the main panel of Fig. 1, with the inset illustrating the low-frequency hydrodynamic regime following Refs. 3 and 36. Our calculation for the collisionless regime is performed at zero temperature. Finite T will affect the low-frequency hydrodynamic regime shown in the inset of Fig. 1, while thermal effects are negligible for $\omega \gg k_B T$. In Fig. 2 we compare $\eta(\omega)/\omega^2$ of Eq. 6 with and without Coulomb interactions, i.e. for $\alpha_0 \neq 0$ and $\alpha_0 = 0$, respectively, in the collisionless regime. Coulomb corrections significantly suppress the viscosity in the regime $\omega \ll D$.

Within the hydrodynamic theory of Galilean-invariant systems, dissipation affects the energy flow and the momentum flux as quantified by the thermal conductivity and the two viscosities, respectively[4]. In particular, the shear viscosity, η, describes the tendency towards a uniform flow and can be directly related[35,37–39] to the nonlocal optical conductivity, $\sigma(\boldsymbol{q},\omega)$. In contrast, the electronic hydrodynamics in graphene describes the energy flow[13] while dissipation affects the electric current (as well as the momentum flux). Here the shear viscosity determines the nonlocal thermal conductivity, $\kappa(\boldsymbol{q},\omega)$. At charge neutrality, the electric current and energy current are completely disentangled and orthogonal[13,20], while the electrical conductivity is independent of viscosity[1,6,13,20]. The mutual independence of the electric and energy current manifests itself in the maximal violation of the Wiedemann-Franz law[9]. Far away from the neutrality point (i.e. for $|\mu| \ll T$), the electronic system in graphene behaves similarly to a Fermi liquid[6,7]. Here the energy current and the electric current are collinear and hence proportional to each other. Both currents now depend on both η[13,39] such that the above relation between $\sigma(\boldsymbol{q},\omega)$ and η (as well as the Wiedemann-Franz law[9]) is restored. Finally, we note that the roles of frequency and temperature in this picture are not equivalent: the macroscopic currents can only be entagled by the collision integral. In the collisionless regime, the electric and energy currents remain orthogonal at charge neutrality; $\sigma(\boldsymbol{q},\omega)$ remains independent of η even if $|\mu| \ll \omega$.

Focusing on the charge neutrality point in graphene, we derive the relation between the viscosity and thermal conductivity using the Kubo formula approach of Ref. 38 which we generalize to multi-component Dirac systems described by a pseudo-spin. This insight may be relevant not only to graphene, but also for other multi-band materials such as topological insulators, their surface states, Lieb lattices, and related systems.

Having briefly described our main results, we now describe the organization of the remainder of this paper. In section II we develop the formalism for the dynamic viscoelastic response of graphene in the collisionless regime generalizing the framework of Ref. 38 to systems with a pseudo-spin structure, including a formal proof of Eq. (4). Section III is devoted to the calculation of the dynamic viscosity of pure graphene at charge neutrality in the collisionless regime and it is split in two parts. In the first part, Section III A, we introduce the RG procedure which

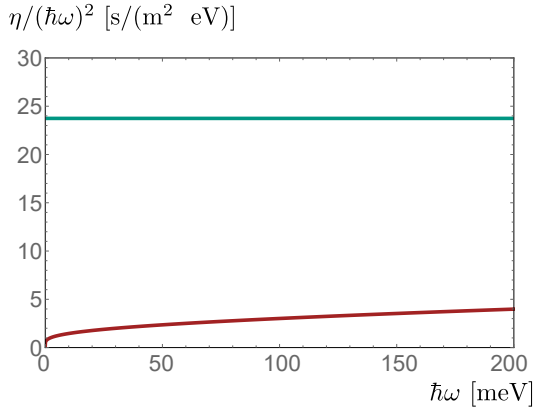

FIG. 2. (Color Online) The effect of electron-electron interaction on the shear viscosity of pure graphene at charge neutrality in the high-frequency collisionless regime. The green line shows $\eta^{(0)}(\omega)/(\hbar\omega)^2$ for free Dirac fermions, see Eq. (61). The red curve shows our result (6) for the dynamical shear viscosity, $\eta(\omega)/(\hbar\omega)^2$, including the interaction effects also shown in Fig. 1.

justifies our perturbative calculation of the dynamic viscosity. In the second part, Section III B, we derive the first term in Eq.(6) which corresponds to the viscosity of non-interacting Dirac fermions, while the interaction correction is calculated in the following subsection. In Section IV we derive the relation between $\eta_{\alpha\beta\gamma\delta}(\omega)$ and $\kappa(\boldsymbol{q},\omega)$ and in Section V we provide concluding remarks.

II. VISCOELASTIC RESPONSE OF THE ELECTRON FLUID

In this Section, we establish a general formalism for the dynamical viscosity by generalizing the approach of Bradlyn *et al.*[38] to multi-band systems with a pseudo-spin structure. In graphene, the pseudo-spin appears due to the sublattice structure of the honeycomb lattice. The low-energy electronic excitations are described by a spinor

$$\psi(\boldsymbol{x}) = \begin{pmatrix} \psi_A(\boldsymbol{x}) \\ \psi_B(\boldsymbol{x}) \end{pmatrix}, \tag{7}$$

comprising the annihilation operators of electrons belonging to the sublattice A or B. In terms of the spinors, the effective low-energy Hamiltonian of pure graphene at charge neutrality is

$$H_{\Omega(t)} = H_{0,\Omega(t)} + H_{\mathrm{int},\Omega(t)}\,, \tag{8a}$$

$$H_{0,\Omega(t)} = v \int\limits_{\Omega(t)} d^d x \psi^\dagger(\boldsymbol{x})\, \boldsymbol{\sigma}\cdot\hat{\boldsymbol{p}}\, \psi(\boldsymbol{x})\,, \tag{8b}$$

$$H_{\mathrm{int},\Omega(t)} = \frac{1}{2}\int\limits_{\Omega(t)} d^d x d^d y \psi^\dagger(\boldsymbol{x})\psi^\dagger(\boldsymbol{y})V(\boldsymbol{x}-\boldsymbol{y})\psi(\boldsymbol{y})\psi(\boldsymbol{x}), \tag{8c}$$

where $\Omega(t)$ describes a time dependent domain within which the electronic systems is assumed to be confined and the dimensionality d is given by $d=2$ for graphene. For simplicity we also use $\Omega(t)$ to denote the volume of this domain. Here v denotes the bare velocity, $\hat{\boldsymbol{p}}$ is the momentum operator, and $\boldsymbol{\sigma}$ is the vector of the Pauli matrices acting in the pseudo-spin space. The additional valley and spin degrees of freedom give rise to an overall degeneracy factor $N=4$ in the viscosity. The electrons interact by the Coulomb law, $V(\boldsymbol{x}-\boldsymbol{y}) = e^2/(4\pi\bar{\epsilon}|\boldsymbol{x}-\boldsymbol{y}|)$.

A. Strain generators for systems with pseudo-spin

Following Ref. 38, we analyze generic coordinate transformations, $\boldsymbol{x}\to\boldsymbol{x}' = \boldsymbol{x}+\boldsymbol{u}(\boldsymbol{x},t)$, which are realized in terms of a homogeneous but time-dependent invertible $d\times d$ matrix $\widehat{\Lambda}(t)$ with a positive determinant via

$$\boldsymbol{x}' = \widehat{\Lambda}(t)^T\boldsymbol{x}. \tag{9}$$

The matrix $\widehat{\Lambda}(t)$ can be expressed in terms of the strain tensor $\hat{\varepsilon}(t)$ of Eq. (2):

$$\widehat{\Lambda}(t) = e^{\hat{\varepsilon}(t)}. \tag{10}$$

Indeed, for small strain we have $\boldsymbol{x}' \approx (\hat{1}+\hat{\varepsilon}^T)\boldsymbol{x}$ with the displacement $\boldsymbol{u}(\boldsymbol{x}) = \hat{\varepsilon}^T\boldsymbol{x}$ and we recover Eq. (2).

Usually, the viscous dynamics is expressed in terms of the response to a velocity gradient. This follows from the relation

$$\frac{\partial v_\delta}{\partial x_\gamma} = \frac{\partial \varepsilon_{\gamma\delta}}{\partial t}. \tag{11}$$

The coordinates x'_α can be strained due to rotations, shear, or compressions. All transformations should adiabatically connect to the unit matrix, which implies the abovementioned restriction $\det\widehat{\Lambda} > 0$.

1. *Uniform compressions*

In order to illustrate the more general case of the next paragraph we first consider uniform compressions which represent a physical system with a time-dependent volume $\Omega(t)$ that preserves its shape and orientation. Our goal is to express the dynamics of $H_{\Omega(t)}$ in terms of a Hamiltonian with a fixed volume Ω_0 and additional perturbations. For homogeneous compressions we write for the transformation matrix:

$$\widehat{\Lambda}(t) = e^{\varepsilon(t)}\hat{1}\,, \tag{12}$$

where the strain tensor is diagonal, $\hat{\varepsilon} = \varepsilon\hat{1}$. The trace of the strain tensor, $\mathrm{Tr}\,\hat{\varepsilon} = d\varepsilon$, determines the relative volume change, $\Omega(t) = e^{d\varepsilon(t)}\Omega_0$ (in the case of graphene $d = 2$).

By requiring that canonical anticommutation relations are preserved, we find the form of the electron field operator after the transformation

$$\psi_\varepsilon(\boldsymbol{x}) = e^{d\varepsilon(t)/2}\psi\left(e^{\varepsilon(t)}\boldsymbol{x}\right). \tag{13}$$

The same transformation can be expressed in terms of a unitary operator

$$\psi_\varepsilon(\boldsymbol{x}) = U(t)\psi(\boldsymbol{x}), \qquad U(t) = e^{-i\varepsilon(t)\mathrm{Tr}\hat{\mathcal{L}}}. \tag{14}$$

The infinitesimal generator $\hat{\mathcal{L}}$ was introduced in Ref. 38 as the "strain generator". The explicit form of the strain generator can be inferred from the requirement that the two forms of the transformation yield identical results[38]. For uniform compressions, the strain generator is diagonal and is given by

$$\mathcal{L}_{\alpha\alpha} = \frac{i}{2} + ix_\alpha\frac{\partial}{\partial x_\alpha}. \tag{15}$$

Since Eq. (14) describes a time-dependent transformation, we obtain the additional contribution to the Hamiltonian

$$\delta H_t = -i\int d^dx\psi^\dagger(\boldsymbol{x},t)U(t)\left[\partial_t U^{-1}(t)\right]\psi(\boldsymbol{x},t).$$

Finally, for arbitrary functions of the momentum or position operators, $f(\boldsymbol{p})$ or $g(\boldsymbol{x})$, respectively, it holds

$$U^{-1}f\left(e^{-\varepsilon(t)}\boldsymbol{p}\right)U = f(\boldsymbol{p}),$$

$$U^{-1}g\left(e^{\varepsilon(t)}\boldsymbol{x}\right)U = g(\boldsymbol{x}).$$

Combining the above expressions, we express the Hamiltonian of a system with time-dependent volume as

$$H_{\Omega(t)} = H_{\Omega_0} - \int d^dx\psi^\dagger(\boldsymbol{x})\frac{\partial\varepsilon}{\partial t}\sum_\alpha\mathcal{L}_{\alpha\alpha}\psi(\boldsymbol{x}), \tag{16}$$

where H_{Ω_0} is the Hamiltonian with a fixed volume Ω_0. Thus, we see that the time-dependent compression can be "gauged away" and yields a form of the Hamiltonian that can be treated within the usual Kubo formalism, see section II C.

We note that the internal spinor structure of the fermion field did not play any role in the above analysis of uniform compressions. However, in our subsequent discussion of arbitrary dynamical strain this will no longer be the case.

2. *Arbitrary dynamical strain*

Now we study arbitrary strain fields, such that $\hat{\Lambda}(t)$ in Eq. (9) is an arbitrary matrix with positive determinant. Following Ref. 38, the transformation of the field operators takes the form

$$\psi_\varepsilon(\boldsymbol{x}) = \sqrt{\det\Lambda}\psi\left(\Lambda^T\boldsymbol{x}\right), \tag{17}$$

where the factor $\sqrt{\det\Lambda}$ ensures the proper canonical commutation relation (i.e., normalization).

For an infinitesimal change from $\hat{\varepsilon}$ to $\hat{\varepsilon} + \delta\hat{\varepsilon}$ we find

$$\frac{\partial}{\partial\varepsilon_{\alpha\beta}}\psi_\varepsilon(\boldsymbol{x}) = \frac{\delta_{\alpha\beta}}{2}\psi_\varepsilon(\boldsymbol{x}) + x'_\alpha\frac{\partial}{\partial x'_\beta}\psi_\varepsilon(\boldsymbol{x}). \tag{18}$$

Here the first term stems from the change in the determinant, while the second term is the derivative with respect to the coordinates $\boldsymbol{x}'$. For infinitesimal changes we may set $\hat{\varepsilon} = 0$ on the right side so that there is no distinction between the two sets of coordinates in the second term. As a result, the infinitesimal strain transformation can be expressed as

$$\begin{aligned}\psi_\varepsilon(\boldsymbol{x}) &= \psi(\boldsymbol{x}) + \sum_{\alpha\beta}\varepsilon_{\alpha\beta}\left.\frac{\partial\psi_\varepsilon(\boldsymbol{x})}{\partial\varepsilon_{\alpha\beta}}\right|_{\varepsilon=0}, \\ &= \left[1 - i\sum_{\alpha\beta}\varepsilon_{\alpha\beta}\mathcal{L}_{\alpha\beta}\right]\psi(\boldsymbol{x}),\end{aligned} \tag{19}$$

with

$$\mathcal{L}_{\alpha\beta} = ix_\alpha\frac{\partial}{\partial x_\beta} + \frac{i}{2}\delta_{\alpha\beta} = -\frac{1}{2}\left\{x_\alpha, p_\beta\right\}, \tag{20}$$

playing the role of the generators of this transformation and generalizing Eq. (15).

Extending these arguments to finite displacements[38], we arrive at the natural generalization of Eq. (14)

$$\psi_\varepsilon(\boldsymbol{x}) = U_\mathcal{L}(t)\psi(\boldsymbol{x}), \quad U_\mathcal{L}(t) = e^{-i\mathrm{Tr}\left(\hat{\varepsilon}^T\hat{\mathcal{L}}\right)}. \tag{21}$$

The form of the strain generators (20) can also be established[38] by considering the transformations of the coordinate and momentum operators,

$$\Lambda^T\boldsymbol{x} = U_\mathcal{L}\boldsymbol{x}U_\mathcal{L}^{-1}, \quad \Lambda^{-1}\boldsymbol{p} = U_\mathcal{L}\boldsymbol{p}U_\mathcal{L}^{-1},$$

which lead to the commutation relations

$$[\mathcal{L}_{\mu\nu}, x_\alpha] = i\delta_{\alpha\nu}x_\mu, \quad [\mathcal{L}_{\mu\nu}, p_\alpha] = -i\delta_{\alpha\mu}p_\nu,$$

satisfied by Eq. (20). The resulting transformation of the momentum operator is

$$U_\mathcal{L}p_\alpha U_\mathcal{L}^{-1} = p_\alpha + \varepsilon_{\alpha\beta}p_\beta. \tag{22}$$

We now recall that the generic coordinate transformations (9) also include spatial rotations. This implies that

the infinitesimal generators (20) are related to the angular momentum. For fermion fields without internal degrees of freedom, the usual (orbital) angular momentum is determined by the antisymmetric part of the strain generator[38], $L_\alpha = -\varepsilon_{\alpha\beta\gamma}\mathcal{L}_{\beta\gamma} = \varepsilon_{\alpha\beta\gamma}x_\beta p_\gamma$. However, as is well-known from standard field theory[40], the proper generators of infinitesimal rotations are the operators of total angular momentum. In the case of graphene, two-dimensional in-plane rotations are generated by the component of the total angular momentum orthogonal to the graphene sheet[41]. Since both sublattices are affected by the rotations, the total angular momentum of the Dirac fermions in graphene includes the pseudo-spin.

A natural form of the Hermitian operator that corresponds to strain transformations in pseudo-spin space is

$$\mathcal{S}_{\alpha\beta} = \frac{i}{8}\left[\sigma_\alpha, \sigma_\beta\right] = -\frac{1}{4}\varepsilon_{\alpha\beta\gamma}\sigma_\gamma, \tag{23}$$

which yields the desired relation to the pseudo-spin contribution to the angular momentum, $S_\alpha = -\varepsilon_{\alpha\beta\gamma}\mathcal{S}_{\beta\gamma}$. The tensor $\mathcal{S}_{\alpha\beta}$ is asymmetric. The only possible choice for a symmetric contribution would be proportional to $\{\sigma_\alpha, \sigma_\beta\} = 2\delta_{\alpha\beta}\sigma_0$, which is trivial in pseudo-spin space. For the unitary transformation in pseudo-spin space we find therefore

$$U_{\mathcal{S}} = e^{-i\mathrm{Tr}\left(\hat{\varepsilon}\hat{\mathcal{S}}\right)} \quad \Rightarrow \quad e^{i(\varepsilon_{xy}-\varepsilon_{yx})\sigma_z/2}\,,$$

where the latter expression is specific for $d = 2$.

The preceding arguments show that the correct strain generator of graphene is

$$\mathcal{J}_{\alpha\beta} = \mathcal{L}_{\alpha\beta} + \mathcal{S}_{\alpha\beta} = -\frac{1}{2}\left\{x_\alpha, p_\beta\right\} + \frac{i}{8}\left[\sigma_\alpha, \sigma_\beta\right], \tag{24}$$

such that the transformation matrix is given by

$$U = U_{\mathcal{S}}U_{\mathcal{L}} = e^{-i\mathrm{Tr}\left(\hat{\varepsilon}\hat{\mathcal{J}}\right)}. \tag{25}$$

Generalizing the above arguments for the case of uniform compressions, we arrive at the following form of the Hamiltonian in a general time-dependent domain, $\Omega\,(t)$,

$$H_{\Omega(t)} = H_{\Omega_0} - \int d^dx \sum_{\alpha\beta}\frac{\partial\varepsilon_{\alpha\beta}}{\partial t}\psi^\dagger(\boldsymbol{x})\mathcal{J}_{\alpha\beta}\psi(\boldsymbol{x}). \tag{26}$$

Thus, a time dependent strain field couples to the strain generator $\mathcal{J}_{\alpha\beta}$ that affects the coordinates and pseudo-spin structure. This result will enable us to determine the proper (symmetric) stress tensor and the Kubo formula for the viscosity of the Dirac fermions in graphene.

B. Momentum conservation and stress tensor

Having determined the form of graphene's strain tensor $\varepsilon_{\beta\alpha}(\boldsymbol{x}, t)$ and its coupling to the electron fluid, taking into account the sublattice structure of the honeycomb lattice, our next task is to identify the stress tensor $\tau_{\beta\alpha}(\boldsymbol{x}, t)$. The linear-response relationship between these tensors, given above in Eq. (3), then defines the viscosity tensor.

To obtain the stress tensor, we begin by recalling that, in a translationally invariant system, momentum is conserved and the operators

$$G_\alpha = -i\int d^dx\ \psi^\dagger(\boldsymbol{x}, t)\partial_\alpha\psi(\boldsymbol{x}, t) \tag{27}$$

of the α-th component of the total momentum commute with the Hamiltonian. Momentum conservation can also be expressed by the continuity equation

$$\partial_t g_\alpha(\boldsymbol{x}, t) + \partial_\beta\tau_{\beta\alpha}(\boldsymbol{x}, t) = 0, \tag{28}$$

where $g_\alpha(\boldsymbol{x}, t)$ is the momentum density

$$g_\alpha(\boldsymbol{x}, t) = -i\psi^\dagger(\boldsymbol{x}, t)\partial_\alpha\psi(\boldsymbol{x}, t), \tag{29}$$

and $\tau_{\alpha\beta}(\boldsymbol{x}, t)$ is the momentum flux or stress tensor.

The choice (29) of the momentum density is, however, not unique[42,43]: adding a contribution acting as a surface term in the integration of Eq. (27) does not change the total momentum. In the standard field theory[42,43] this freedom is used to bring the canonical stress tensor to a symmetric form that is typically assumed in calculations of the viscosity tensor[39] (using an asymmetric stress tensor leads to results that are explicitly incorrect).

In what follows, we modify the momentum density (29) (preserving the total momentum) to[43]

$$g_\alpha(\boldsymbol{x}, t) = \frac{i}{4}\left\{\left[\partial_\alpha\psi^\dagger(\boldsymbol{x}, t) + \boldsymbol{\nabla}\psi^\dagger(\boldsymbol{x}, t)\cdot\boldsymbol{\sigma}\sigma_\alpha\right]\psi(\boldsymbol{x}, t)\right.$$
$$\left. - \psi^\dagger(\boldsymbol{x}, t)\left[\partial_\alpha\psi(\boldsymbol{x}, t) + \sigma_\alpha\boldsymbol{\nabla}\psi(\boldsymbol{x}, t)\cdot\boldsymbol{\sigma}\right]\right\}, \tag{30}$$

in order to derive a symmetric form of $\tau_{\alpha\beta}(\boldsymbol{x}, t)$. The latter can be found by considering the long-wavelength limit of the continuity equation (28). Indeed, applying a Fourier transformation with respect to the spatial coordinates we may write Eq. (28) in the form

$$\partial_t g_\alpha(\boldsymbol{q}, t) - iq_\beta\tau_{\beta\alpha}(\boldsymbol{q}, t) = 0.$$

Expanding the Fourier-transformed momentum density $g_\alpha(\boldsymbol{q}, t)$ for small $\boldsymbol{q}$, we find

$$g_\alpha(\boldsymbol{q}, t) = \int d^dx\ e^{i\boldsymbol{q}\cdot\boldsymbol{x}}g_\alpha\left(\boldsymbol{x}, t\right)\,, \tag{31}$$
$$\approx g_\alpha\left(0, t\right) + iq_\beta\int d^dx\ \psi^\dagger\left(\boldsymbol{x}, t\right)$$
$$\times\left[x_\beta\left(-i\frac{\partial}{\partial x_\alpha}\right) + \frac{1}{4}\epsilon_{\beta\alpha\gamma}\sigma_\gamma\right]\psi\left(\boldsymbol{x}, t\right) + \ldots.$$

To leading order in small $\boldsymbol{q}$, this formula implies conservation of the total momentum $\partial_t g_\alpha\left(\boldsymbol{0}, t\right) = \partial_t G_\alpha\left(t\right) = 0$, while the first subleading order reveals

$$\partial_t\mathcal{J}_{\alpha\beta} = -T_{\alpha\beta}, \tag{32}$$

where

$$T_{\alpha\beta} = \tau_{\alpha\beta}\left(\boldsymbol{q}=\boldsymbol{0}\right) = \int d^d x\, \tau_{\alpha\beta}(\boldsymbol{x}),$$

is the integrated stress tensor and $\mathcal{J}_{\alpha\beta}$ is the stress generator of Eq. (24). As a result, the commutator of the stress generator with the Hamiltonian yields the explicitly symmetric stress tensor

$$T_{\alpha\beta} = -i\left[H, \mathcal{J}_{\alpha\beta}\right]. \tag{33}$$

We postpone evaluating this commutator until after we obtain the Kubo formula expression for graphene's viscosity. Before proceeding to this task we note that in the case of a rotationally invariant system, the resulting stress tensor is equivalent to the Belinfante-Rosenfeld stress-energy tensor in the usual Dirac theory[44,45]. The approach presented here, however, has the advantage that it may also be applied to anisotropic systems such as the anisotropic Dirac fluids studied in Ref. 17.

C. Kubo formalism for the viscosity tensor

We now proceed with the development of the Kubo formalism for the dynamic viscosity of graphene. To make our presentation self-contained, we begin by summarizing the usual linear response theory[46,47]. Consider a system subjected to an external, time-dependent perturbation

$$\delta H = -\sum_j A_j F_j\left(t\right), \tag{34}$$

characterized by the operators A_j and time dependent functions $F_j\left(t\right)$. Within linear response, the expectation values $\langle A_i\rangle_t$ acquire an additional contribution

$$\delta\langle A_i\rangle_t = \int_{-\infty}^{\infty} dt \sum_j G_{ij}(t-t')F_j(t'), \tag{35}$$

where

$$G_{ij}(t) = -i\theta(t)\langle[A_i(t), A_j(0)]\rangle,$$

is the retarded Green's function. In addition, one may make use of the Kubo identity

$$i\left[A(t),\rho\right] = \rho\int_0^\beta d\tau \dot{A}(t-i\tau),$$

perform a Fourier transformation and partial integration, and obtain

$$G_{ij}(\omega) = \frac{i}{\omega+i0^+}\left[\chi_{ij}(\omega)-\chi_{ij}^T\right], \tag{36}$$

where

$$\chi_{ij}(t-t') = -i\theta(t-t')\left\langle\left[A_i(t), \dot{A}_j(t')\right]\right\rangle,$$

and

$$\chi_{ij}^T = \left.\frac{\partial\langle A_i\rangle}{\partial F_j^{\rm stat}}\right|_{F_j^{\rm stat}=0},$$

is the isothermal susceptibility due to an external static field $F_j^{\rm stat}$ coupling to $\dot{A}_j$ in the Hamiltonian[46].

Now we apply the above Kubo formalism to the viscosity tensor defined by the linear response relation

$$\delta\langle\tau_{\alpha\beta}\rangle_t = \langle\tau_{\alpha\beta}\rangle_{\boldsymbol{x}'} - \langle\tau_{\alpha\beta}\rangle_{\boldsymbol{x}} = \int_{-\infty}^{\infty} dt \sum_{\gamma\delta}\eta_{\alpha\beta\gamma\delta}(t-t')\frac{\partial\varepsilon_{\gamma\delta}}{\partial t}, \tag{37}$$

where $\langle\tau_{\alpha\beta}\rangle_{\boldsymbol{x}'(\boldsymbol{x})}$ indicates the stress tensor averaged over the system with the deformed or undeformed coordinates, respectively.

The time dependent strain field $\varepsilon_{\alpha\beta}(t)$ couples to the system by means of Eq. (26). At the same time, the integrated stress tensor is proportional to the time derivative of $\mathcal{J}_{\alpha\beta}$, see Eqs. (32), (33). Here one has to distinguish between the integrated stress tensor $T_{\alpha\beta}$ and the local stress tensor $\tau_{\alpha\beta}(\boldsymbol{q}=0)$ which are connected via

$$\langle T_{\alpha\beta}\rangle = \int_\Omega d^d x\langle\tau_{\alpha\beta}(\boldsymbol{x})\rangle = V\langle\tau_{\alpha\beta}(\boldsymbol{q}=0)\rangle. \tag{38}$$

In order to determine the viscosity, we need to calculate $\langle\tau_{\alpha\beta}\rangle_{\boldsymbol{x}'}$, i.e., the expectation value of the stress tensor in the deformed coordinate system, see Eq. (37). Using the perturbation defined in Eq. (26) we may determine the expectation value of the integrated stress tensor

$$\langle T_{\alpha\beta}\rangle_{\boldsymbol{x}'} = \langle T_{\alpha\beta}\rangle_{\boldsymbol{x}} + \int_{-\infty}^{\infty} dt\; X_{\alpha\beta\gamma\delta}\,\frac{\partial\varepsilon_{\gamma\delta}}{\partial t}\,, \tag{39}$$

where the correlation function $X_{\alpha\beta\gamma\delta}(\omega)$ is defined as

$$X_{\alpha\beta\gamma\delta}(\omega) = \frac{-1}{i(\omega+i0^+)}\left(\frac{\partial\left\langle T_{\alpha\beta}\right\rangle}{\partial\varepsilon_{\gamma\delta}} + C_{\alpha\beta\gamma\delta}(\omega)\right)_{\boldsymbol{x}}, \tag{40}$$

with $C_{\alpha\beta\gamma\delta}(\omega)$ being the Fourier transform of the stress-stress correlation function

$$C_{\alpha\beta\gamma\delta}(t-t') = i\theta(t-t')\langle[T_{\alpha\beta}(t), T_{\gamma\delta}(t')]\rangle, \tag{41}$$

previously introduced in Eq. (3).

The correlation function $X_{\alpha\beta\gamma\delta}(\omega)$ can be related to the local stress tensor using Eq. (38) and the transformation law $V_{\boldsymbol{x}'} = V_{\boldsymbol{x}}\exp(\mathrm{Tr}\,\hat{\varepsilon})$,

$$\langle\tau_{\alpha\beta}\rangle_{\boldsymbol{x}'} = (1-\delta_{\gamma\delta}\varepsilon_{\gamma\delta})\langle\tau_{\alpha\beta}\rangle_{\boldsymbol{x}} + \frac{1}{V_{\boldsymbol{x}'}}\int_{-\infty}^{\infty} dt\;\left(X_{\alpha\beta\gamma\delta}\right)_{\boldsymbol{x}}\frac{\partial\varepsilon_{\gamma\delta}}{\partial t}. \tag{42}$$

Hence, the viscosity tensor has the form

$$\eta_{\alpha\beta\gamma\delta}(t) = X_{\alpha\beta\gamma\delta}(t) - \delta_{\delta\gamma}\langle\tau_{\alpha\beta}\rangle_{\boldsymbol{x}}\theta(t). \tag{43}$$

Now we use the identity

$$\varepsilon_{\gamma\delta}(t) = \int_{-\infty}^{t} dt' \; \frac{\partial\varepsilon_{\gamma\delta}}{\partial t'} = \int_{-\infty}^{\infty} dt' \; \theta(t)\frac{\partial\varepsilon_{\gamma\delta}}{\partial t'},$$

to perform the Fourier transformation of the viscosity tensor

$$\begin{aligned}\eta_{\alpha\beta\gamma\delta}(\omega) &= X_{\alpha\beta\gamma\delta}(\omega) - \frac{\langle\tau_{\alpha\beta}\rangle_{\boldsymbol{x}}\delta_{\gamma\delta}}{i(\omega+i0^+)}\,, \\ &= X_{\alpha\beta\gamma\delta}(\omega) - \frac{\delta_{\gamma\delta}P}{i(\omega+i0^+)}, \end{aligned} \tag{44}$$

where we have used the fact that the averaged stress tensor defines the pressure of the system

$$\langle\tau_{\alpha\beta}\rangle_{\boldsymbol{x}} = P\,\delta_{\alpha\beta}.$$

Finally, using Eq. (36) we express the dynamic viscosity as

$$\eta_{\alpha\beta\gamma\delta}\,(\omega) = \frac{C^T_{\alpha\beta\gamma\delta} - C_{\alpha\beta\gamma\delta}(\omega)}{i(\omega+i0^+)}, \tag{45}$$

where

$$C^T_{\alpha\beta\gamma\delta} = -\left.\frac{d\langle\tau_{\alpha\beta}\rangle}{d\varepsilon^{\rm stat}_{\gamma\delta}}\right|_{\varepsilon_{\alpha\beta}=0},$$

is the isothermal elastic constant (we have added a term $-T_{\gamma\delta}\varepsilon^{\rm stat}_{\gamma\delta}$ with static strain $\varepsilon^{\rm stat}_{\gamma\delta}$ to the Hamiltonian). The above argument constitutes a formal proof of Eq. (4).

III. DYNAMIC VISCOSITY OF GRAPHENE

In this Section, we use the Kubo formula Eq. (45) to evaluate the dynamic viscosity tensor of pure graphene at charge neutrality and in the collisionless regime. Since we work at finite frequencies, we can drop the delta-function part of Eq. (45) to arrive at

$$\eta_{\alpha\beta\gamma\delta}(\omega) = \frac{\mathrm{Im}\; C_{\alpha\beta\gamma\delta}(\omega)}{\omega}. \tag{46}$$

Thus, we only need to compute the Fourier transform of the correlation function (41). In doing this, we shall combine perturbation theory with the renormalization group (RG) in order to arrive at the result Eq. (6).

A. RG procedure

We begin by describing our RG procedure, which will allow us to determine the shear viscosity of interacting graphene in the collisionless regime. The small parameter justifying our calculation is the renormalized coupling constant at frequency ω, $\alpha(\omega)$, which is small at $\omega \ll D$, where D is the bandwidth of graphene (unlike the bare coupling constant, which is not small, with $\alpha_0 = e^2/(\hbar v\bar{\epsilon}) \approx 2.2$ for the vacuum case $\bar{\epsilon} = 1$).

To obtain the RG equations for the coupling parameter and for the shear viscosity we perform a leading order RG analysis, which shows that the Fermi velocity of graphene is renormalized by the Coulomb interaction and diverges logarithmically with growing RG flow $b = e^l$ where l is the RG flow parameter[21,51]:

$$v \to v\left(1 + \frac{\alpha}{4}\ln b\right). \tag{47}$$

This leads to the fact that the flow equation of the coupling constant is given by

$$\frac{d\alpha(b)}{d\ln b} = -\frac{1}{4}\alpha(b)^2. \tag{48}$$

which is solved by the following expression for the coupling constant

$$\alpha(b) = \frac{\alpha_0}{1 + \frac{\alpha_0}{4}\ln(D/b)}\,. \tag{49}$$

Simultaneously, the frequency is renormalized by the scaling factor $Z_\omega(b)$ which has the form

$$Z_\omega(b) = \left[1 + \frac{\alpha}{4}\ln b\right] b^{-1}. \tag{50}$$

Next we consider the behavior of the viscosity tensor under the RG flow. In distinction to the electrical conductivity, which is scale invariant in two dimensions, the viscosity has a finite scaling dimension which is given by the dimensionality d of the system, a result that follows from momentum conservation and the isotropy of space[49]. Thus we have the rigorous relation

$$\eta_{\alpha\beta\gamma\delta}\,(\omega,\alpha_0) = b^{-d}\eta_{\alpha\beta\gamma\delta}\left(Z_\omega\,(b)^{-1}\,\omega, \alpha\,(b)\right). \tag{51}$$

The physical viscosity at the bare value α_0 of the coupling constant can be expressed in terms of the viscosity at a higher frequency and a weaker coupling constant, since $\alpha\,(b>1) < \alpha_0$. Scaling is expected to stop at the scale b^* where the renormalized frequency equals the band width: $\omega/Z_\omega\,(b^*) = D$. This leads to

$$b^*\,(\omega) = \frac{D}{\omega}\left(1 + \frac{\alpha_0}{4}\ln\frac{D}{\omega}\right)\,, \tag{52}$$

and $\alpha\,(\omega) = \alpha\,(b^*\,(\omega))$ given in Eq. (51). If we insert this result into Eq. (51) we obtain

$$\eta_{\alpha\beta\gamma\delta}\,(\omega,\alpha_0) = \frac{\omega^2\eta_{\alpha\beta\gamma\delta}\,(D,\alpha\,(\omega))}{D^2\left(1 + \frac{\alpha_0}{4}\ln\frac{D}{\omega}\right)^2}. \tag{53}$$

Our remaining task is to determine the high-frequency viscosity at weak coupling. For $\eta_{\alpha\beta\gamma\delta}\,(D,\alpha\,(\omega))$ we can

then perform a perturbation theory calculation to obtain

$$\eta_{\alpha\beta\gamma\delta}\left(D,\alpha\left(\omega\right)\right)=\eta^{(0)}_{\alpha\beta\gamma\delta}\left(D\right)\left(1+C_{\eta}\alpha\left(\omega\right)+\cdots\right), \quad (54)$$

where $\eta^{(0)}_{\alpha\beta\gamma\delta}\left(D\right)$ is the viscosity of non-interacting electrons at frequency $\omega=D$ and C_η a numerical coefficient of order unity that we will determine in the next section.

Equation (51) implies that electron-electron interactions impact graphene's viscosity in two ways: Firstly, by the overall prefactor $b_*^{-d}=b_*^{-2}$. As we shall see, this yields the frequency-dependent Fermi velocity factor in Eq. (6). Secondly, interactions enter via the renormalized viscosity $\eta_{\alpha\beta\gamma\delta}(D,\alpha(b^*))$ on the right side of Eq. (51). Much of our subsequent calculations will involve computing this to leading perturbative order in $\alpha(b^*)=\alpha(\omega)$. This will require computing the correlation function $C_{\alpha\beta\gamma\delta}$ within perturbation theory. Below, we call the zeroth order, e.g., $\mathcal{O}(\alpha^0)$, and first order, $\mathcal{O}(\alpha^1)$, contributions to this quantity as $C^{(0)}_{\alpha\beta\gamma\delta}$ and $C^{(1)}_{\alpha\beta\gamma\delta}$, respectively.

Diagrammatically, these contributions are depicted in Figs. 3 and 4. The response of free Dirac fermions, $C^{(0)}_{\alpha\beta\gamma\delta}$, is shown in Fig. 4, panel (a). Notably, this contribution has nothing to do with dissipation (which is absent in any non-interacting system), but rather describes the nonlocal energy-flow response of Dirac fermions to an external time-dependent perturbation. The correlation function $C^{(0)}_{\alpha\beta\gamma\delta}$ is evaluated in Section III B.

Obtaining the perturbative contribution to the dynamical shear viscosity, $C^{(1)}_{\alpha\beta\gamma\delta}$, requires computing the leading-order Feynman diagrams in the interaction parameter, as shown in Fig. 4, panels (b)-(e). The corresponding calculation is presented in Section III C.

B. Free Dirac fermions

We begin with the zeroth order calculation, which corresponds to the collisionless dynamic viscosity of non-interacting graphene. The Matsubara stress-stress correlation function of a system of non-interacting Dirac fermions is given by[39]

$$C^{(0)}_{\alpha\beta\gamma\delta}(i\Omega) \quad (55)$$

$$=T\sum_{\omega}\int\frac{d^2k}{(2\pi)^2}\mathrm{Tr}\left[G_{\boldsymbol{k},i\omega}\mathcal{T}^{(0)}_{\alpha\beta}(\boldsymbol{k})G_{\boldsymbol{k},i(\omega+\Omega)}\mathcal{T}^{(0)}_{\gamma\delta}(\boldsymbol{k})\right],$$

where $\mathcal{T}^{(0)}_{\alpha\beta}$ are the vertex operators corresponding to the stress tensor (33), see Fig. 3, and $G_{\boldsymbol{k},i\omega}$ are the Matsubara Green's functions

$$G_{\boldsymbol{k},i\omega}=-\frac{(\mathrm{i}\omega\sigma_0+v\boldsymbol{k}\cdot\boldsymbol{\sigma})}{(\omega^2+(vk)^2)}=\frac{1}{2}\sum_{s=\pm1}\frac{\sigma_0+sv\boldsymbol{\sigma}\cdot\boldsymbol{k}/k}{i\omega-vk}, \quad (56)$$

with s being the band index. The corresponding diagram is shown in Fig. 4, panel (a).

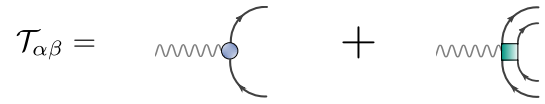

FIG. 3. (Color online) Diagrammatic representation of the stress tensor vertex. The left vertex describes the non-interacting stress tensor (60). The right vertex describes the interaction part of the stress tensor (66).

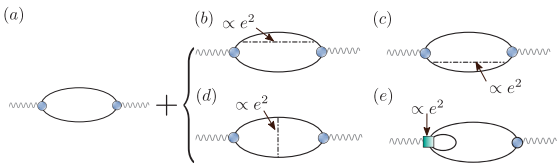

FIG. 4. (Color online) Feynman diagrams for the correlation function of the stress tensor. The diagram (a) describes the dynamic viscosity of non-interacting Dirac fermions, while the remaining diagrams determine the leading order correction due to the Coulomb interaction. in the main text the diagrams (b) and (c) are referred to as the self-energy diagrams, diagram (d) – the vertex diagram, and diagram (e) as the "honey diagram" that includes the interaction correction to the stress tensor.

Given that the strain generator (24) is a combination of the orbital and pseudo-spin parts, we evaluate the two corresponding contributions to the stress tensor separately. The orbital contribution is given by

$$T^{\mathcal{L},(0)}_{\alpha\beta}=-i[\mathcal{L}_{\alpha\beta},H_0]=\int\frac{d^2k}{(2\pi)}\psi^\dagger_{\boldsymbol{k},t}\sigma_\alpha k_\beta\psi_{\boldsymbol{k},t}, \quad (57)$$

where $\psi_{\boldsymbol{k},t}$ is the spinor (7) in momentum space and time domain. Note that this expression is explicitly not symmetric. However, adding the pseudo-spin contribution

$$T^{\mathcal{S},(0)}_{\alpha\beta}=-i[\mathcal{S}_{\alpha\beta},H_0]=\frac{1}{2}\int\frac{d^2k}{(2\pi)}\psi^\dagger_{\boldsymbol{k},t}(\sigma_\beta k_\alpha-\sigma_\alpha k_\beta)\psi_{\boldsymbol{k},t}, \quad (58)$$

where H_0 is defined by Eq. (8b), we arrive at the symmetric expression of the stress tensor

$$T^{(0)}_{\alpha\beta}=-i[\mathcal{J}_{\alpha\beta},H_0]=\frac{1}{2}\int\frac{d^2k}{(2\pi)}\psi^\dagger_{\boldsymbol{k},t}(k_\alpha\sigma_\beta+k_\beta\sigma_\alpha)\psi_{\boldsymbol{k},t}. \quad (59)$$

The corresponding vertices (see Fig. 3)

$$\mathcal{T}^{(0)}_{\alpha\beta}=\frac{1}{2}(k_\alpha\sigma_\beta+k_\beta\sigma_\alpha), \quad (60)$$

are time-independent and we may perform the sum over the Matsubara frequencies in Eq. (55) to obtain:

$$T\sum_{\omega}\frac{1}{i\omega-s_1vk}\frac{1}{i\omega+i\Omega-s_2vk}=\frac{n_F(s_1vk)-n_F(s_2vk)}{(s_1-s_2)vk+i\Omega},$$

where $n_F(\omega) = \frac{1}{e^{\omega/T}+1}$ is the Fermi function.

After analytical continuation, $i\Omega \to \omega + i\delta$, the imaginary part of this expression is given by a δ-function,

$$\mathrm{Im}\frac{1}{(s_1-s_2)vk+\omega+i\delta} = -i\pi\delta(\omega-(s_1-s_2)vk),$$

reflecting the expected behavior that only interband transitions, $s_1 \neq s_2$, contribute to the dynamic viscosity (with $\omega > 0$).

The remaining integration is straightforward. As a result, we obtain for the dynamical shear viscosity of non-interacting Dirac fermions in pure graphene at charge neutrality:

$$\eta^{(0)}(\omega) = \frac{\hbar}{64v^2}\omega^2, \tag{61}$$

which corresponds to the shear viscosity $\eta(\omega)$ of the standard expression (5) for the viscosity tensor $\eta_{\alpha\beta\gamma\delta}$.

The above calculation demonstrates the importance of the pseudo-spin structure of the fermionic excitations in multi-band systems (in other words, of the interband transitions). Evaluating the viscosity tensor using the orbital part of the stress-tensor (57) only, one arrives at $\eta_{\alpha\beta\gamma\delta}$ with the tensor structure that explicitly violates Eq. (5). The reason for this incorrect result is that Eq. (32) is not fulfilled. The fact that physically correct results correspond to the symmetric stress tensor (59) is well recognized in literature[39,42,43] based on the known result (5) for rotationally invariant systems. The problem becomes more difficult in the anisotropic case[17], where one does not have the guidance of the known result. Our derivation of the strain generators and symmetric stress tensor allows us to establish the structure of the viscosity tensor from first principles without relying on any phenomenological assumptions.

C. Dynamic viscosity of interacting graphene

We now consider the Coulomb interaction correction to the viscosity correlation function, which we denote as $C^{(1)}_{\alpha\beta\gamma\delta}$. Drawing on past experience of the calculation of the optical conductivity[23,24,31,32] which has shown the resulting diagrams to be separately divergent, we modify the Coulomb interaction to

$$V(\boldsymbol{r},\boldsymbol{r}') = \frac{e^2 r_0^{-\delta}}{|\boldsymbol{r}-\boldsymbol{r}'|^{1-\delta}}\,, \tag{62}$$

and take the limit $\delta \to 0$ at the end. Here, r_0 is a length scale introduced to preserve the units of the system at finite δ. In the case of the optical conductivity calculation, this modification provides a "soft cut-off" regularization of the logarithmically divergent diagrams, such that the divergent contributions of the self-energy and vertex diagrams cancel out yielding the finite result (1). The Fourier transform of the modified Coulomb potential (62) is given by

$$V(\boldsymbol{q}) = \frac{2\pi\alpha_\delta}{|\boldsymbol{q}|^{1+\delta}}, \tag{63}$$

where $\alpha_\delta = \alpha\, r_0^{-\delta} 2^\delta \Gamma[(1+\delta)/2]/\Gamma[(1-\delta)/2]$. We note that the reason for the introduction of the exponent δ instead of using a screened Coulomb potential is that we are evaluating the shear viscosity at the charge neutrality point and in the collisionless regime, $\omega\tau_{ee} \gg 1$, which leads to the fact that the calculation can be performed at $T = 0$. Hence, there is no charge density to screen the Coulomb potential.

In addition, the validity of the present regularization scheme is ensured by the fact that it reproduces the same value for the coefficient $\mathcal{C}_\sigma$ in the optical conductivity (1) found in the Dirac model and the tight-binding model of graphene[32].

In distinction to the charge current, the momentum current of our system contains single-particle contributions, Eq. (59), and many-body contributions. The latter take into account the flow of momentum by interaction effects. Our first task is to evaluate this *interaction part of the stress tensor*

$$T^{(\mathrm{int})}_{\alpha\beta}(\boldsymbol{r}) = -i[\mathcal{J}_{\alpha\beta}, H_{\mathrm{int}}]. \tag{64}$$

Explicitly, we find[50]

$$T^{(\mathrm{int})}_{\alpha\beta}(\boldsymbol{r}) = \int d^2r_1 d^2r_2 \psi^\dagger(\boldsymbol{r_1})\psi^\dagger(\boldsymbol{r_2})\psi(\boldsymbol{r_2})\psi(\boldsymbol{r_1})(r_{1\alpha}-r_{2\alpha})\nabla_{\boldsymbol{r_2}\beta}V(\boldsymbol{r_1},\boldsymbol{r_2}) \tag{65}$$

$$= \frac{(1-\delta)r_0^{-\delta}}{2}\int d^2r_1 d^2r_2 \psi^\dagger(\boldsymbol{r_1})\psi^\dagger(\boldsymbol{r_2})\psi(\boldsymbol{r_2})\psi(\boldsymbol{r_1})\frac{(r_{1\alpha}-r_{2\alpha})(r_{1\beta}-r_{2\beta})}{|\boldsymbol{r_1}-\boldsymbol{r_2}|^{3-\delta}}.$$

The integrated stress-tensor can be obtained by calculating the zero-momentum Fourier component of $T^{(\mathrm{int})}_{\alpha\beta}(\boldsymbol{r})$,

$$T^{(\mathrm{int})}_{\alpha\beta}(\boldsymbol{q}=\boldsymbol{0},\tau) = \frac{1-\delta}{2}r_0^{-\delta}2^{1-\delta}\pi\frac{\Gamma[(3+\delta)/2]}{\Gamma[(3-\delta)/2]}\int\frac{d^2l}{(2\pi)^2}\frac{l_\alpha l_\beta}{|\boldsymbol{l}|^{3+\delta}}n(\boldsymbol{l},\tau)n(-\boldsymbol{l},\tau), \tag{66}$$

with the density operators in momentum space,

$$n(\boldsymbol{l},\tau) = \int\frac{d^2p}{(2\pi)^2}\psi^\dagger_{\boldsymbol{p}}(\tau)\psi_{\boldsymbol{p}+\boldsymbol{l}}(\tau)\,. \tag{67}$$

The remaining calculation of the interaction correc-

tion to the dynamic viscosity amounts to the evaluation of the four Feynman diagrams shown in Fig. 4, panels (b)-(e). In contrast to the similar calculation of the optical conductivity[23,24,31,32], these include an additional diagram, see Fig. 4, panel (e), describing the correlation between the interaction part of the stress tensor $T^{(\mathrm{int})}_{\alpha\beta}$ and the non-interacting part $T^{(0)}_{\alpha\beta}$. In what follows we will refer to this diagram as the "honey diagram", since the high viscosity of classical fluids such as honey arises mostly due to the strong interaction between the fluid molecules leading to a large contribution of $T^{(\mathrm{int})}_{\alpha\beta}$.

Computing the contributions of different diagrams separately, we arrive at the interaction correction to the correlation function in the form

$$C^{(1)}_{\alpha\beta\gamma\delta} = C^{(1,bc)}_{\alpha\beta\gamma\delta} + C^{(1,d)}_{\alpha\beta\gamma\delta} + C^{(1,e)}_{\alpha\beta\gamma\delta}. \tag{68}$$

Given the tensor structure (5) it is sufficient to evaluate just one component of the viscosity tensor. Focusing on $C^{(1)}_{xyxy}$, we write the three different contributions to the correlation function as

$$C^{(1,bc)}_{xyxy}(i\Omega) = -2N\int\frac{\omega}{2\pi}\int\frac{d^2p}{(2\pi)^2}\mathrm{Tr}\left[G_{p,i(\omega+\Omega)}\mathcal{T}^{(0)}_{xy}(\boldsymbol{p})G_{p,i\omega}\Sigma(\boldsymbol{p})G_{p,i\omega}\mathcal{T}^{(0)}_{xy}(\boldsymbol{p})\right], \tag{69}$$

with the self-energy

$$\Sigma(\boldsymbol{p}) = \int\frac{d\omega'}{2\pi}\int\frac{d^2k}{(2\pi)^2}\frac{2\pi\alpha_\delta}{|\boldsymbol{p}-\boldsymbol{k}|^{1+\delta}}G_{p,i\omega'} = \phi(\boldsymbol{p})\boldsymbol{p}\cdot\boldsymbol{\sigma}, \qquad \phi(\boldsymbol{p}) = \alpha r_0^{-\delta}\frac{2^\delta\Gamma(\frac{\delta}{2})}{8\Gamma(\frac{4-\delta}{2})}p^{-\delta}, \tag{70}$$

$$C^{(1,d)}_{xyxy}(i\Omega) = N\alpha_\delta\int\frac{d\omega d\omega'}{(2\pi)^2}\int\frac{d^2p}{(2\pi)^2}\frac{d^2k}{(2\pi)^2}\frac{2\pi}{|\boldsymbol{p}-\boldsymbol{k}|^{1+\delta}}\mathrm{Tr}\left[G_{p,i\omega}\mathcal{T}^{(0)}_{xy}(\boldsymbol{p})G_{p,i(\omega+\Omega)}G_{k,i(\omega'+\Omega)}\mathcal{T}^{(0)}_{xy}(\boldsymbol{k})G_{k,i\omega'}\right], \tag{71}$$

$$C^{(1,e)}_{xyxy}(i\Omega) = 4N\int\frac{d\omega}{(2\pi)^2}\int\frac{d^2k}{(2\pi)^2}\mathrm{Tr}\left[G_{\boldsymbol{k},i\omega}\mathcal{T}^{(\mathrm{int})}_{xy}(\boldsymbol{k})G_{\boldsymbol{k},i(\omega+\Omega)}\mathcal{T}^{(0)}_{xy}(\boldsymbol{k})\right]. \tag{72}$$

Self-energy and vertex diagrams. The dynamic viscosity (46) is determined by the imaginary part of $C^{(1)}_{\alpha\beta\gamma\delta}$ (after analytical continuation to real frequencies, $i\Omega\to\omega+i\delta$). In the self-energy and vertex contributions, Eqs. (69) and (71), the imaginary part is "less divergent" than the real part. This can be seen by using the Kramers-Kronig relations to analyze the Matsubara frequency dependence of the bare bubble, which has the form $C_{\alpha\beta\gamma\delta}\propto a\Lambda^2+b\Lambda\Omega^2+i\mathcal{N}\Omega^3$ where Λ is an ultraviolet cutoff (proportional to the bandwidth) and a, b, and $\mathcal{N}$ are numerical coefficients. The imaginary part is determined by the third term of this expression and is free of any ultra-violet divergences. Anticipating that $C^{(1,bc)}_{xyxy}(i\Omega)$ and $C^{(1,d)}_{xyxy}(i\Omega)$ will have the same form, we proceed by carefully subtracting the first two contributions in these expressions that are proportional to Λ^2 and Λ. For the functions analytically continued to the real frequency axis, we find for the self-energy diagram

$$\begin{aligned}\mathrm{Im}\ C^{(1,bc)}_{xyxy}/\omega &= -\alpha\frac{4^{\delta-5}(\delta-4)\omega^{-\delta}r_0^{-\delta}\Gamma(\delta/2)}{\cos(\pi\delta/2)\Gamma(2-\delta/2)}\omega^2\\ &= \left[\frac{1}{2\delta}+\mathcal{N}_{self}-\frac{\ln(r_0\omega/4)}{2}+\mathcal{O}(\delta)\right]\alpha(\omega)\eta^{(0)}(\omega),\end{aligned} \tag{73}$$

with $\mathcal{N}_{self}=1/8-\gamma/2$ and for the vertex diagram

$$\begin{aligned}&\mathrm{Im}\ C^{(1,d)}_{xyxy}/\omega\\ &= \left[-\frac{1}{4\delta}+\mathcal{N}_{vertex}+\frac{\ln(r_0\omega/4)}{4}+\mathcal{O}(\delta)\right]\alpha(\omega)\eta^{(0)}(\omega),\end{aligned} \tag{74}$$

with $\mathcal{N}_{vertex}=-193/80+(\gamma+2\pi)/4$, where the above expressions are valid for small δ. The details of the calculation to determine the numerical coefficients $\mathcal{N}_{self}$ and $\mathcal{N}_{vertex}$ can be found in the appendix.

The self-energy and vertex diagrams, which describe single-particle propagation, are still divergent for $\delta\to 0$. In contrast to the case of the optical conductivity (with similar diagrams), these divergences do not cancel when summed, indicating that the final "honey" diagram (panel e of Fig. 4) must contribute additional divergent contributions.

Honey diagram. The above divergence of the self-energy and vertex diagrams at $\delta\to 0$ will be canceled if the remaining "honey" diagram has the form

$$\begin{aligned}&\mathrm{Im}\ C^{(1,e)}_{xyxy}/\omega\\ &= \left[-\frac{1}{4\delta}+\mathcal{N}_{honey}+\frac{\ln(r_0\omega/4)}{4}+\mathcal{O}(\delta)\right]\alpha(\omega)\ \eta^{(0)}(\omega).\end{aligned} \tag{75}$$

To show that this is indeed the case we begin with the Matsubara expression of the honey diagram, which con-

tains one noninteracting stress tensor vertex and one vertex from the interacting part of the stress tensor:

$$C^{(1,e)}_{xyxy}(i\Omega) = -2\pi(1-\delta)r_0^{-\delta}2^{3+\delta}\frac{\Gamma[(3+\delta)/2]}{\Gamma[(3-\delta)/2]}T^2\sum_{\omega\omega'}\int\frac{d^2l}{(2\pi)^2}\frac{d^2k}{(2\pi)^2}\frac{l_\alpha l_\beta}{|\boldsymbol{l}|^{3+\delta}}\mathrm{Tr}\left[G_{\boldsymbol{k}+\boldsymbol{l},i\omega'}G_{\boldsymbol{k},i(\omega+\Omega)}\mathcal{T}^{(0)}_{xy}G_{\boldsymbol{k},i\omega}\right]. \quad (76)$$

Summing over the frequencies, we find

$$C^{(1,e)}_{xyxy}(i\Omega) = (1-\delta)r_0^{-\delta}2^{3+\delta}\pi\frac{\Gamma[(3+\delta)/2]}{\Gamma[(3-\delta)/2]}\frac{1}{(2\pi)^4}\int_0^\infty dk\int_0^\infty dl\int_0^{2\pi}d\alpha\int_0^{2\pi}d\beta\frac{k^3l^{1-\delta}\sin 2\alpha\cos 2\beta\sin(\alpha-\beta)}{(4k^2+\Omega^2)\sqrt{k^2+2kl\cos(\alpha-\beta)+l^2}}. \quad (77)$$

Now, we analytically continue the obtained function to real frequencies and evaluate the imaginary part of the correlation function. Here we make use of the identity

$$\frac{1}{4k^2+\Omega^2}\to\frac{\mathcal{P}}{4k^2-\omega^2}+\frac{i\pi}{4\omega}\delta\left(k-\frac{\omega}{2}\right)+\frac{i\pi}{4\omega}\delta\left(k+\frac{\omega}{2}\right), \quad (78)$$

where $\mathcal{P}$ denotes the principal value. The resulting imaginary part of the correlation function is given by

$$\frac{\mathrm{Im}C^{(1,e)}_{xyxy}}{\omega} = \alpha\frac{2^{2\delta-8}(\delta-1)\omega^{-\delta}r_0^{-\delta}\Gamma(\delta/2)}{\Gamma(3-\delta/2)}\omega^2 = \left[-\frac{1}{4\delta}+\mathcal{N}_{honey}+\frac{\ln(r_0\omega/4)}{4}+\mathcal{O}(\delta)\right]\alpha(\omega)\eta^{(0)}(\omega), \quad (79)$$

with $\mathcal{N}_{honey} = 1/16+\gamma/4$, which has the exact form as Eq. (75) and thus cancels the divergence of the self-energy and vertex diagrams. As a result, the perturbative expression for the conductivity, on the right side of Eq. (51), has the form of Eq. (5) with

$$\eta(D,\alpha(\omega)) = \eta^{(0)}(D)\left[1+\mathcal{C}_\eta\alpha(\omega)\right], \quad (80)$$

and the correction coefficient

$$\mathcal{C}_\eta = \mathcal{N}_{self}+\mathcal{N}_{vertex}+\mathcal{N}_{honey} = \frac{89-20\pi}{40}\approx 0.65. \quad (81)$$

When we use Eq. (61) and insert this into the RG equation Eq. (53), we finally arrive at Eq. (6).

Thus, in contrast to the case of the optical conductivity of graphene, the dynamic viscosity of graphene reveals significant interaction corrections. These are due to the velocity renormalization but also due to the interaction correction $\mathcal{C}_\eta$ that is much larger than the corresponding correction $\mathcal{C}_\sigma = 0.01$ in the optical conductivity.

IV. CONNECTION BETWEEN VISCOSITY AND THERMAL CONDUCTIVITY

In this Section, we relate graphene's dynamic viscosity to its nonlocal (momentum dependent) energy flow expressed in terms of the thermal conductivity. Our derivation is similar to one presented by Bradlyn *et al.*[38] relating the viscosity to the momentum-dependent conductivity tensor $\sigma_{\nu\beta}(\boldsymbol{q},\omega)$ in a Galilean invariant (GI) system. The relation derived in Ref. 38 relies on two facts. Firstly, the continuity equation Eq. (28) allows one to relate correlation functions of the momentum to strain correlation functions (and, hence, the viscosity tensor). Following Bradlyn *et al.*, the relation is (with $\omega^+ = \omega+i0^+$, and in the limit of $\boldsymbol{q}\to 0$):

$$(\omega^+)^2\int_0^\infty dt\,\mathrm{e}^{i\omega^+t}\int d^2x\mathrm{e}^{-i\boldsymbol{q}\cdot\boldsymbol{x}}\langle[g_\nu(\boldsymbol{x},t),g_\beta(0,0)]\rangle$$
$$= q_\lambda q_\rho\omega^+\left(\eta_{\lambda\nu\rho\beta}(\omega)+\frac{i\kappa^{-1}}{\omega^+}\delta_{\lambda\nu}\delta_{\rho\beta}\right), \quad (82)$$

with κ being the compressibility.

The second fact used by Bradlyn *et al.* is that, in a system with GI, the momentum density is proportional to the particle current, so that the momentum correlation function can be related to a current correlation function which, within the Kubo formalism, determines the optical conductivity. This then leads to the relation

$$\sigma_{\nu\beta}(\boldsymbol{q},\omega) = \frac{in\delta_{\nu\beta}}{m\omega^+}+\frac{q_\lambda q_\rho}{m(\omega^+)^2}\left(\eta_{\lambda\nu\rho\beta}(\omega)+\frac{i\kappa^{-1}}{\omega^+}\delta_{\lambda\nu}\delta_{\rho\beta}\right), \quad (83)$$

connecting the electrical conductivity to the viscosity tensor in a GI system (equivalent to Eq.(4.9) of Ref. 38 in the limit of $B\to 0$). Here, n is the average charge density.

In graphene, the lack of GI implies that the momentum current is not proportional to the charge current and the relation (83) does not hold. However, since Eq. (82) still holds, it is natural to ask if it can be used to derive an alternate relation connecting the viscosity tensor to a response function of graphene. To do this, we note that the momentum density Eq. (30) is proportional to

the energy current in graphene[6,7,13]. We can see this by considering the noninteracting energy density operator

$$\varepsilon(\boldsymbol{x}) = -\frac{iv}{2}\left[\psi^\dagger(\boldsymbol{x})\boldsymbol{\sigma}\cdot\boldsymbol{\nabla}\psi(\boldsymbol{x}) - \left[\boldsymbol{\sigma}\cdot\boldsymbol{\nabla}\psi^\dagger(\boldsymbol{x})\right]\psi(\boldsymbol{x})\right], \quad (84)$$

which satisfies the continuity equation

$$\boldsymbol{\nabla}\cdot\boldsymbol{Q}(\boldsymbol{x},t) + \partial_t\varepsilon(\boldsymbol{x},t) = 0, \quad (85)$$

with $\boldsymbol{Q}(\boldsymbol{x},t) = v^2\boldsymbol{g}(\boldsymbol{x},t)$, so that, indeed, the energy current is directly proportional to the momentum density Eq. (30).

Using this connection along with Eq. (82), we now proceed to relate the nonlocal thermal conductivity to the viscosity tensor. Following Luttinger[48], we add a time-dependent perturbation to our system Hamiltonian,

$$H_1 = \int d^2x\, \varepsilon(\boldsymbol{x})\chi(\boldsymbol{x},t), \quad \chi(\boldsymbol{x},t) = e^{-i\omega^+ t}\chi(\boldsymbol{x}),$$

allowing us to incorporate, e.g. a local temperature gradient, $\boldsymbol{\nabla}\chi(\boldsymbol{x}) = -\boldsymbol{\nabla}T/T$ (with ω a frequency scale of the temperature oscillations). Following the standard linear response theory[47], we obtain the frequency-dependent heat current $\langle Q_\alpha\rangle = -\kappa_{\alpha\beta}(\boldsymbol{q},\omega)\partial_\beta T$ with the thermal conductivity tensor

$$\kappa_{\alpha\beta}(\boldsymbol{q},\omega) = \frac{v^4}{iT\omega^+}K_{\alpha\beta}(\boldsymbol{q},\omega), \quad (86)$$

$$K_{\alpha\beta}(\boldsymbol{q},\omega) \equiv -\int dt\, e^{i\omega^+ t}\int d^2x\, e^{-i\boldsymbol{q}\cdot\boldsymbol{x}}\langle[g_\alpha(\boldsymbol{x},t), g_\beta(0,0)]\rangle,$$

in terms of a Fourier-transformed correlation function $K_{\alpha\beta}(\boldsymbol{q},\omega)$ of the momentum density. Now using Eq. (82) and taking the large ω limit (in which we may neglect the term proportional to the inverse compressibility), we finally arrive at

$$\kappa_{\alpha\beta}(\boldsymbol{q},\omega) = -\frac{v^4}{T(\omega^+)^2}q_\lambda q_\rho\eta_{\lambda\alpha\rho\beta}(\omega), \quad (87)$$

the desired relation between the frequency-dependent viscosity tensor and the nonlocal thermal conductivity.

Dropping the infinitesimal part of the frequency and plugging in our main result, Eq. (6), we obtain (assuming the standard frequency-dependent renormalization of the velocity):

$$\kappa_{\alpha\beta}(\boldsymbol{q},\omega) = -\frac{\hbar v(\omega)^2q^2}{64T}\delta_{\alpha\beta}\left(1 + \mathcal{C}_\eta\alpha(\omega)\cdots\right), \quad (88)$$

for the nonlocal thermal or energy-flow response of graphene in the collisionless regime.

V. CONCLUSIONS

We determined the elastic response of graphene in the collisionless regime and related it to the nonlocal energy flow response of the system. In doing so we extended the theoretical framework of Bradlyn *et al.*[38] in which the viscosity was derived using strain generators to systems with pseudo-spins and showed that the pseudopsin also contributes to the shear viscosity in the collisionless regime and cannot be neglected.

In particular, we demonstrated that the Coulomb interaction between the quasiparticles of graphene has a sizable influence on the shear viscosity of graphene in the collisionless regime. Therefore, the self-energy diagram, the vertex diagram and the honey diagram were evaluated using a soft cut-off on the Coulomb potential. The momentum flux of the system is then governed by comparable single-particle and many-particle contributions. The correction coefficient in first order of the coupling constant determined out of the sum of these Feynman diagrams is given by $\mathcal{C} = (89 - 20\pi)/40 \approx 0.65$. The influence of this value of the correction coefficient can be seen in Fig. 1.

VI. ACKNOWLEDGEMENT

This work was performed in part at the Aspen Center for Physics, which is supported by National Science Foundation grant PHY-1607611. J.M.L. thanks the Carl-Zeiss-Stiftung for financial support. DES also acknowledges support from NSF grant No. DMR-1151717. BNN acknowledges support from the MEPhI Academic Excellence Project, Contract No. 02.a03.21.0005

Appendix A: Correction coefficient of the viscosity in the collisionless regime

Here, we give a detailed presentation of the calculation of the different Feynman diagrams contributing to the correction coefficient $\mathcal{C}_\eta$. These diagrams are the *self-energy diagram*, the *vertex diagram* and the *honey diagram*. To evaluate the different diagrams, we introduce a soft cut-off to the Coulomb interaction $V_\delta(\boldsymbol{q}) = 2\pi\alpha_\delta/|\boldsymbol{q}|^{1+\delta}$ where the small parameter δ regularizes the integrals. The coupling constant α_δ is defined as $\alpha_\delta = \alpha_0\, r_0^{-\delta}\zeta_\delta$ with $\zeta_\delta = \frac{2^\delta\Gamma\left(\frac{1+\delta}{2}\right)}{\Gamma\left(\frac{1-\delta}{2}\right)}$, where we introduced the length scale r_0 in such a way that the dimensionality of Coulomb interaction remains unchanged.

1. The self-energy diagram

We start with the evaluation of the self energy which is defined as

$$\Sigma(\boldsymbol{k}) = \int\frac{d\omega}{2\pi}\frac{d^2p}{(2\pi)^2}\frac{2\pi\alpha_\delta}{|\boldsymbol{p}-\boldsymbol{k}|^{1+\delta}}G_{p,i\omega} = \phi(\boldsymbol{k})\boldsymbol{k}\cdot\boldsymbol{\sigma}, \quad (A1)$$

with

$$\phi(\boldsymbol{k}) = \mathcal{A}k^{-\delta} = \alpha_0 r_0^{-\delta} \frac{2^\delta \Gamma(\delta/2)}{8\Gamma(2-\delta/2)} k^{-\delta}. \tag{A2}$$

The correlation function of the self-energy diagram is given by

$$C^{(1,bc)}_{xyxy}(i\Omega) = -8 \int\limits_P \mathrm{Tr}\left[G_{\boldsymbol{p},i(\omega+\Omega)} \mathcal{T}^{(0)}_{xy}(\boldsymbol{p}) G_{\boldsymbol{p},i\omega} \Sigma(\boldsymbol{p}) G_{\boldsymbol{p},i\omega} \mathcal{T}^{(0)}_{xy}(\boldsymbol{p})\right]$$

$$= -\alpha_0 r_0^{-\delta} \frac{1}{4} \frac{2^\delta \Gamma(\delta/2)}{\Gamma(2-\delta/2)} \int \frac{d^2k}{(2\pi)^2} \frac{d\omega}{2\pi} \frac{p^{-\delta}}{(k^2+(\omega+\Omega)^2)} \frac{\mathrm{Tr}(\mathcal{B})}{(k^2+\omega^2)^2}, \tag{A3}$$

with

$$\mathrm{Tr}(\mathcal{B}) = -2k_x(k_x+k_y)\left(k_x^4 + k_x^2\left[\omega(\omega+2\Omega) - 10k_y^2\right] + k_y^2\left[5\left(k_y^2+\omega^2\right) + 2\omega\Omega\right]\right). \tag{A4}$$

After performing the frequency integral and the integration over the angle, we obtain

$$C^{(1,bc)}_{xyxy}(i\Omega) = \alpha_0 \int\limits_0^\infty dk \frac{2^{\delta-4}\Gamma(\delta/2) k^{4-\delta}\left(4k^2-\Omega^2\right)}{\pi\Gamma(2-\delta/2)\left(4k^2+\Omega^2\right)^2}. \tag{A5}$$

In order to determine the numerical coefficient of the imaginary part of the correlation function $C^{(1,bc)}_{xyxy}(i\Omega)$, we have to calculate the difference

$$f^{(1,bc)}_{xyxy}(i\Omega) = \frac{C^{(1,bc)}_{xyxy}(i\Omega) - C^{(1,bc)}_{xyxy}(0)}{\Omega^2} = -\alpha_0 \int\limits_0^\infty dk \frac{2^{\delta-6}\Gamma\left(\frac{\delta}{2}\right) k^{2-\delta}\left(12k^2+\Omega^2\right)}{\pi\Gamma\left(2-\frac{\delta}{2}\right)\left(4k^2+\Omega^2\right)^2}, \tag{A6}$$

and

$$\frac{f^{(1,bc)}_{xyxy}(i\Omega) - f^{(1,bc)}_{xyxy}(0)}{\Omega} = \alpha_0 \int\limits_0^\infty dk \frac{2^{\delta-8}\Omega\Gamma(\delta/2) k^{-\delta}\left(20k^2+3\Omega^2\right)}{\pi\Gamma(2-\delta/2)\left(4k^2+\Omega^2\right)^2} = -\alpha_0 \frac{4^{\delta-5}(\delta-4)\Omega^{-\delta}\Gamma(\delta/2)}{\cos(\pi\delta/2)\Gamma(2-\delta/2)},$$

$$\approx \frac{\alpha_0}{128\ \delta} + \alpha_0 \frac{-4\ln(r_0\Omega) - 4\gamma + 1 + 4\ln(4)}{512} + \mathcal{O}(\delta), \tag{A7}$$

where in the last step we expanded the expression for small δ. The self-energy diagram diverges upon taking the limit $\delta \to 0$. The other two Feynman diagrams are going to cancel this divergence.

2. The vertex diagram

In this section we focus on the vertex diagram. The vertex diagram is defined by the following correlation function

$$C^{(1,d)}_{xyxy}(\mathrm{i}\Omega) = -\int \frac{d^2p}{(2\pi)^2} \frac{d\omega}{2\pi} \int \frac{d^2k}{(2\pi)^2} \frac{d\omega'}{2\pi} \frac{2\pi\alpha_\delta}{|\boldsymbol{p}-\boldsymbol{k}|^{1+\delta}} \mathrm{Tr}\left[G_{\boldsymbol{p},\mathrm{i}\omega} \mathcal{T}^{(0)}_{xy}(\boldsymbol{p}) G_{\boldsymbol{p},i(\omega+\Omega)} G_{\boldsymbol{k},i(\omega'+\Omega)} \mathcal{T}^{(0)}_{xy}(\boldsymbol{k}) G_{\boldsymbol{k},i\omega'}\right]. \tag{A8}$$

After inserting the corresponding expressions of the Green's functions and the energy-stress tensor and performing the two frequency integrals, we find

$$C^{(1,d)}_{xyxy}(i\Omega) = -\int \frac{d^2p}{(2\pi)^2} \frac{d^2q}{(2\pi)^2} \frac{2\pi\alpha_\delta}{|\boldsymbol{p}-\boldsymbol{q}|^{1+\delta}} \frac{2}{pq\left(4p^2+\Omega^2\right)\left(4q^2+\Omega^2\right)}$$

$$\times \left\{p^2\left[p_x q_x\left(q^2+q_x^2-3q_y^2\right) + p_y q_y\left(q^2-3q_x^2+q_y^2\right)\right]\right.$$

$$+p_x^3 q_x\left(q^2+q_x^2-3q_y^2\right) + p_x^2\left[\Omega^2\left(q_y^2-q_x^2\right) - 3p_y q_y\left(q^2-3q_x^2+q_y^2\right)\right]$$

$$\left.-3p_x p_y^2 q_x\left(q^2+q_x^2-3q_y^2\right) + p_y^2\left[p_y q_y\left(q^2-3q_x^2+q_y^2\right) + \Omega^2(q_x-q_y)(q_x+q_y)\right]\right\}. \tag{A9}$$

Next, we subtract the zero-frequency part from the above expression to obtain

$$f^{(1,d)}_{xyxy}(i\Omega) = \frac{C^{(1,d)}_{xyxy}(i\Omega) - C^{(1,d)}_{xyxy}(0)}{\Omega^2}. \tag{A10}$$

To finally determine the contribution to the correction coefficient, we have to subtract again the zero-frequency part which yields

$$\frac{f^{(1,d)}_{xyxy}(i\Omega) - f^{(1,d)}_{xyxy}(0)}{\Omega} = Q_1 + Q_2 + Q_3, \tag{A11}$$

where Q_1 and Q_2 are convergent for $\delta = 0$, whereas the integral Q_3 is divergent for $\delta \to 0$. The explicit expression of these three integrals are

$$Q_1 = -\frac{\alpha_\delta}{2}\frac{\Omega^{-\delta}}{(2\pi)^2}\int_0^\infty \frac{dp}{p(4p^2+1)}\int_0^\infty \frac{dq}{q(4q^2+1)}\int_0^\pi d\varphi \frac{(pq/4)\cos 2\varphi + p^2q^2\cos\varphi\cos 2\varphi}{[p^2+q^2-2pq\cos\varphi]^{(1+\delta)/2}}\,, \tag{A12}$$

$$Q_2 = -\alpha_\delta\frac{\Omega^{-\delta}}{(2\pi)^2}\int_0^\infty \frac{dp}{p(4p^2+1)}\int_0^\infty \frac{dq}{q(4q^2+1)}\int_0^\pi d\varphi \frac{p^3q\cos 2\varphi}{[p^2+q^2-2pq\cos\varphi]^{(1+\delta)/2}}\,, \tag{A13}$$

$$Q_3 = -\frac{\alpha_\delta}{16}\frac{\Omega^{-\delta}}{(2\pi)^2}\int_0^\infty \frac{pdp}{p^2(4p^2+1)}\int_0^\infty \frac{qdq}{q^2(4q^2+1)}\int_0^{2\pi} d\varphi \frac{\cos\varphi\cos 2\varphi[p^2(4p^2+1)+q^2(4q^2+1)]}{[p^2+q^2-2pq\cos\varphi]^{(1+\delta)/2}}\,. \tag{A14}$$

In the following, we demonstrate how the different integrals are evaluated.

a. Calculation of Q_1 Since Q_1 is convergent for $\delta = 0$, we set $\delta = 0$, substitute the momentum variable q by introducing the variable $q = xp$ and obtain the following expression:

$$Q_1 = -\frac{\alpha_\delta}{2}\frac{\Omega^{-\delta}}{(2\pi)^2}\int_0^\infty \frac{dp}{4p^2+1}\int_0^\infty \frac{dx}{4x^2p^2+1}\int_0^\pi d\varphi \frac{(1/4)\cos 2\varphi + xp^2\cos\varphi\cos 2\varphi}{\sqrt{1+x^2-2x\cos\varphi}}. \tag{A15}$$

The integration over p can be done easily using

$$\int_0^\infty \frac{dp}{4p^2+1}\frac{1}{4x^2p^2+1} = \frac{\pi}{4(1+x)}, \qquad \int_0^\infty \frac{dp}{4p^2+1}\frac{p^2}{4x^2p^2+1} = \frac{\pi}{16x(1+x)}. \tag{A16}$$

After performing first the x-integral and than the angle integral, we find

$$Q_1 = -\frac{\alpha_\delta}{240}\,. \tag{A17}$$

b. Calculation of Q_2 Here again, we apply the variable substitution $q = xp$ which leads to the integral

$$Q_2 = -\alpha_\delta\frac{\Omega^{-\delta}}{(2\pi)^2}\int_0^\infty \frac{dpp^{2-\delta}}{4p^2+1}\int_0^\infty \frac{dx}{4x^2p^2+1}\int_0^\pi \frac{d\varphi\cos 2\varphi}{[1+x^2-2x\cos\varphi]^{(1+\delta)/2}} = q\int_0^\infty dx\frac{1-x^{\delta-1}}{x^2-1}\int_0^\pi d\varphi\frac{2\cos^2(\varphi)-1}{[1+x^2-2x\cos\varphi]^{(1+\delta)/2}}, \tag{A18}$$

with

$$q = -\frac{N\alpha_\delta\Omega^{-\delta}}{4(2\pi)^2}\frac{2^{\delta-4}\pi}{\cos(\pi\delta/2)}. \tag{A19}$$

In order to evaluate this integral, we split up the integral in two parts. These two integrals are defined as:

$$Q_{2,a} = 2q\int_0^\infty dx\frac{1-x^{\delta-1}}{x^2-1}\int_0^\pi d\varphi\frac{\cos(\varphi)^2}{[1+x^2-2x\cos\varphi]^{(1+\delta)/2}}, \tag{A20}$$

$$Q_{2,b} = -q\int_0^\infty dx\frac{1-x^{\delta-1}}{x^2-1}\int_0^\pi d\varphi\frac{1}{[1+x^2-2x\cos\varphi]^{(1+\delta)/2}}. \tag{A21}$$

Analysis of $Q_{2,a}$ This integral can be split in a singular and a non-singular contribution $Q_{2,a} = Q^s_{2,a} + Q^{ns}_{2,a}$, where the singular contribution is given by

$$Q^s_{2,a} = 2q \int_0^\infty dx \frac{1-x^{\delta-1}}{x^2-1} \int_0^\pi d\varphi \cos^2\varphi = q\frac{\pi^2}{2}\cot(\pi\delta/2). \tag{A22}$$

Next, the non-singular contribution is analyzed, which is defined as

$$Q^{ns}_{2,a} = Q_{2,a} - Q^s_{2,a} = 2q \int_0^\infty dx \frac{1-x^{\delta-1}}{x^2-1} \int_0^\pi d\varphi \cos^2\varphi \left[\frac{1}{[1+x^2-2x\cos\varphi]^{(1+\delta)/2}} - 1\right]. \tag{A23}$$

Since this integral is convergent for $\delta = 0$, it can be evaluated in this limit. We find

$$Q^{ns}_{2,a} = 2q \int_0^\infty dx \frac{1}{x(1+x)} \int_0^\pi d\varphi \cos^2\varphi \left[\frac{1}{\sqrt{1+x^2-2x\cos\varphi}} - 1\right] = \frac{\pi q}{6}(11 - 6\pi + \ln 4096), \tag{A24}$$

where we first performed the x-integral and then the φ-integral.

Analysis of $Q_{2,b}$ This integral is again split up into a singular and a non-singular contribution. The singular contribution is given by

$$Q^s_{2,b} = -q \int_0^\pi d\varphi \int_0^\infty dx \frac{1-x^{\delta-1}}{x^2-1} = -\frac{\pi^2 q}{2}\cot(\pi\delta/2). \tag{A25}$$

The non-singular part, which is convergent and can be evaluated for $\delta = 0$, reads

$$Q^{ns}_{2,b} = Q_{2,b} - Q^s_{2,b} = -q \int_0^\infty dx \frac{1}{x(1+x)} \int_0^\pi d\varphi \left[\frac{1}{\sqrt{1+x^2-2x\cos\varphi}} - 1\right] = \frac{\pi q}{2}(\pi - 2\ln 4). \tag{A26}$$

Result for Q_2 Combining $Q_{2,a}$ and $Q_{2,b}$, we obtain for the integral Q_2 the following value:

$$Q_2 = Q_{2,a} + Q_{2,b} = Q^{ns}_{2,a} + Q^s_{2,a} + Q^{ns}_{2,b} + Q^s_{2,b} = -\frac{\alpha_\delta \Omega^{-\delta}}{(2\pi)^2} \frac{2^{\delta-4}\pi}{\cos(\pi\delta/2)} \frac{\pi}{6}(11 - 3\pi) \approx -\alpha_0 \left(\frac{22}{768} - \frac{2\pi}{256}\right), \tag{A27}$$

where in the last line we expanded for small δ.

c. Calculation of Q_3 After the variable substitution $p = xq$, we need to evaluate the following integral

$$Q_3 = -\frac{\alpha_\delta \Omega^{-\delta}}{8(2\pi)^2} \int_0^\infty \frac{dq q^{-\delta}}{4q^2+1} \int_0^\infty dx \int_0^{2\pi} d\varphi \frac{x\cos\varphi\cos 2\varphi}{[1+x^2-2x\cos\varphi]^{(1+\delta)/2}}, \tag{A28}$$

which is divergent for $\delta \to 0$. In the following step we use the identity:

$$|\boldsymbol{k}|^{-(1+\delta)} = \frac{1}{\Gamma[(1+\delta)/2]} \int_0^\infty dz \frac{e^{-k^2 z}}{z^{(1-\delta)/2}}, \tag{A29}$$

and obtain

$$Q_3 = -\frac{\alpha_\delta \Omega^{-\delta}}{(2\pi)^2} \frac{2^{1+\delta}\pi}{\Gamma[(1+\delta)/2]\cos(\pi\delta/2)} \int_0^\infty dx \int_0^{2\pi} d\varphi \cos\varphi\cos 2\varphi \int_0^\infty dz \frac{x}{z^{(1-\delta)/2}} e^{-\left(1+x^2-2x\cos\varphi\right)z}, \tag{A30}$$

$$= -\frac{\alpha_\delta \Omega^{-\delta}}{(2\pi)^2} \frac{2^{1+\delta}\pi}{\cos(\pi\delta/2)} \frac{\pi(\delta+2)\Gamma[(1-\delta)/2]\Gamma(\delta/2)}{4\Gamma[(1+\delta)/2]\Gamma(3-\delta/2)} \approx -\frac{\alpha_0}{256\delta} - \frac{\alpha_0(4\ln(r_0\Omega) + 4\gamma - 5 - 8\ln 2)}{1024} + \mathcal{O}(\delta),$$

where in the last line we expanded the above expression for small δ.

d. Result of the vertex diagram Combining all three integrals yields

$$\frac{f^{(1,d)}_{xyxy}(i\Omega)-f^{(1,d)}_{xyxy}(0)}{\Omega}=-\frac{\alpha_0}{256\,\delta}+\frac{\alpha_0(20\ln(\Omega r_0)+40\pi+20\gamma-193-40\ln 2)}{5120}. \tag{A31}$$

The vertex diagram is also divergent for $\delta\to 0$, but does not fully cancel the divergence of the self-energy diagram. A third Feynman diagram is needed to cancel all divergences.

3. The honey diagram

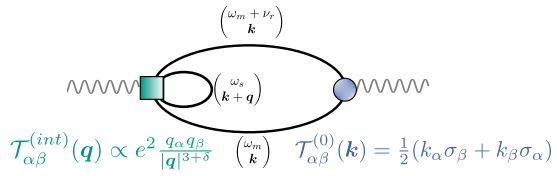

FIG. 5. The honey diagram.

The last diagram contributing to the correction coefficient $\mathcal{C}$ is the *honey diagram*, which takes account of the interacting part of the energy-stress tensor. The correlation function is given by

$$C^{(1,e)}_{xyxy}(\mathrm{i}\Omega)=-(1-\delta)r_0^{-\delta}2^{4+\delta}\pi\frac{\Gamma[(3+\delta)/2]}{\Gamma[(3-\delta)/2]}\int\limits_{\boldsymbol{k},\boldsymbol{l},m,s}\frac{l_\alpha l_\beta}{|\boldsymbol{l}|^{3+\delta}}\mathrm{Tr}\left[G_{\boldsymbol{k}+\boldsymbol{l},i\omega_s}G_{\boldsymbol{k},i(\omega_m+\nu_r)}\mathcal{T}^{(0)}_{xy}(\boldsymbol{k})G_{\boldsymbol{k},i\omega_m}\right]. \tag{A32}$$

This Feynman diagram is depicted in Fig. 5. Inserting the explicit formulas of the Green's function and the stress tensor into the above equation yields

$$C^{(1,e)}_{xyxy}(i\Omega)=-(1-\delta)r_0^{-\delta}2^{3+\delta}\pi\frac{\Gamma[(3+\delta)/2]}{\Gamma[(3-\delta)/2]}\int\limits_{\boldsymbol{k},\boldsymbol{l},m,s}\frac{l_\alpha l_\beta}{|\boldsymbol{l}|^{3+\delta}}\frac{\mathrm{Tr}[\mathcal{A}]}{(\omega'^2+|\boldsymbol{l}+\boldsymbol{k}|^2)(k^2+\omega^2)[k^2+(\omega+\Omega)^2]}, \tag{A33}$$

where the trace is given by

$$\mathrm{Tr}[\mathcal{A}]=-2\left\{(k_x+l_x)k_y\left[-3k_x^2+k_y^2+\omega(\omega+\Omega)\right]+(k_y+l_y)k_x\left[k_x^2-3k_y^2+\omega(\omega+\Omega)\right]+2k_xk_y\omega'(2\omega+\Omega)\right\}. \tag{A34}$$

Next, we perform the two frequency integrations and find

$$C^{(1,e)}_{xyxy}(\mathrm{i}\Omega)=(1-\delta)r_0^{-\delta}\frac{2^{3+\delta}\pi}{(2\pi)^4}\frac{\Gamma[(3+\delta)/2]}{\Gamma[(3-\delta)/2]}\int_0^\infty dk\int_0^\infty dl\int_0^{2\pi}d\alpha\int_0^{2\pi}d\beta\frac{k^3l^{1-\delta}\sin 2\alpha\cos 2\beta\sin(\alpha-\beta)}{(4k^2+\Omega^2)\sqrt{k^2+2kl\cos(\alpha-\beta)+l^2}}. \tag{A35}$$

Upon using Eq. (78), we find that the imaginary part of the correlation function can be cast into the form

$$\mathrm{Im}C^{(1,e)}_{xyxy}(\omega)=(1-\delta)r_0^{-\delta}\frac{2^{3+\delta}\pi}{(2\pi)^4}\frac{\Gamma[(3+\delta)/2]}{\Gamma[(3-\delta)/2]}\int_0^\infty dl\int_0^{2\pi}d\alpha\int_0^{2\pi}d\beta\frac{\pi\omega^2l^{1-\delta}\sin 2\alpha\cos 2\beta\sin(\alpha-\beta)}{16\sqrt{4l^2+4l\omega\cos(\alpha-\beta)+\omega^2}}. \tag{A36}$$

Next, we substitute the angle $\alpha\to\varphi+\beta$ and perform the β integration and obtain

$$\mathrm{Im}C^{(1,e)}_{xyxy}(\omega)=(1-\delta)r_0^{-\delta}\frac{2^{3+\delta}\pi}{(2\pi)^4}\frac{\Gamma[(3+\delta)/2]}{\Gamma[(3-\delta)/2]}\int_0^\infty dl\int_0^{2\pi}d\varphi\frac{\pi^2\omega^2l^{1-\delta}\sin^2\varphi\cos\varphi}{16\sqrt{l^2+l\omega\cos\varphi+\omega^2/4}}. \tag{A37}$$

After using Eq. (A29), we obtain

$$\mathrm{Im}C^{(1,e)}_{xyxy}(\omega)=(1-\delta)r_0^{-\delta}\frac{2^{3+\delta}\pi^{5/2}}{(2\pi)^4}\frac{\Gamma[(3+\delta)/2]}{\Gamma[(3-\delta)/2]}\int_0^\infty dl\int_0^{2\pi}d\varphi\int_0^\infty dz\,\omega^2l^{1-\delta}\sin^2\varphi\cos\varphi\frac{e^{-\left(l^2+l\omega\cos\varphi+\omega^2/4\right)}}{16\sqrt{z}}. \tag{A38}$$

As the last step, we first perform the angle-integration over φ, than the l-integration and at last the z-integration, which leads to

$$\mathrm{Im}C^{(1,e)}_{xyxy}(\omega) = \frac{2^{2\delta-8}(\delta-1)\omega^{3-\delta}\Gamma(\delta/2)}{\Gamma(3-\delta/2)} \approx -\frac{\omega^3}{256\delta} + \omega^3\frac{4\ln(r_0\omega)+4\gamma+1-8\ln 2}{1024} + \mathcal{O}(\delta), \tag{A39}$$

where we expanded the above expression for small δ. The honey diagram is also divergent for $\delta \to 0$. When all three diagrams are summed up, these divergences cancel each other.

4. The correction coefficient

Upon combining all three Feynman diagrams, we find for the correction coefficient $\mathcal{C}_\eta$

$$\mathcal{C}_\eta = \frac{89-20\pi}{40} \simeq 0.65\,. \tag{A40}$$

This is a relatively large correction coefficient and hence, the impact of the Coulomb interaction on the shear viscosity of graphene in the collisionless regime is large.

[1] L. Fritz, J. Schmalian, M. Müller & S. Sachdev, Phys. Rev. B **78**, 085416 (2008).
[2] A. Kashuba, Phys. Rev. B **78**, 085415 (2008).
[3] M. Müller, J. Schmalian & L. Fritz, Phys. Rev. Lett. **103**, 025301 (2009).
[4] L. D. Landau and E. M. Lifshitz, *Fluid Mechanics* (Butterworth-Heinemann, Oxford, UK, 2000).
[5] D. Forster, *Hydrodynamic Fluctuations, Broken Symmetry, and Correlation Functions*, Frontiers in Physics 47, XIX, 326 S., London-Amsterdam-Don Mills-Sydney-Tokyo (1975).
[6] A. Lucas, K. C. Fong, Journal of Physics: Condensed Matter **30**, 053001 (2018).
[7] B. N. Narozhny, I. V. Gornyi, A. D. Mirlin, and J. Schmalian, Ann. d. Physik **529**, 1700043 (2017).
[8] M. Titov, R. V. Gorbachev, B. N. Narozhny, T. Tudorovskiy, M. Schütt, P. M. Ostrovsky, I. V. Gornyi, A. D. Mirlin, M. I. Katsnelson, K. S. Novoselov, A. K. Geim & L. A. Ponomarenko, Phys. Rev. Lett. **111**, 166601 (2013).
[9] J. Crossno, J. K. Shi, K. Wang, X. Liu, A. Harzheim, A. Lucas, S. Sachdev, P. Kim, T. Taniguchi, K. Watanabe, T. A. Ohki & K. C. Fong, Science **351**, 1058 (2016).
[10] F. Ghahari, H.-Y. Xie, T. Taniguchi, K. Watanabe, M. S. Foster & P. Kim, Phys. Rev. Lett. **116**, 136802 (2016).
[11] D. A. Bandurin, I. Torre, R. Krishna Kumar, M. Ben Shalom, A. Tomadin, A. Principi, G. H. Auton, E. Khestanova, K. S. Novoselov, I. V. Grigorieva, L. A. Ponomarenko, A. K. Geim & M. Polini, Science **351**, 1055 (2016).
[12] R. Krishna Kumar, D. A. Bandurin, F. M. D. Pellegrino, Y. Cao, A. Principi, H. Guo, G. H. Auton, M. B. Shalom, L. A. Ponomarenko, G. Falkovich, I. V. Grigorieva, L. S. Levitov, M. Polini & A. K. Geim, Nature Physics **13**, 1182 (2017).
[13] U. Briskot, M. Schütt, I. V. Gornyi, M. Titov, B. N. Narozhny & A. D. Mirlin, Phys. Rev. B **92**, 115426 (2015).
[14] A. Lucas, J. Crossno, K. C. Fong, P. Kim, S. Sachdev, Phys. Rev. B **93,** 075426 (2016).
[15] L. S. Levitov & G. Falkovich, Nature Phys. **12**, 672 (2016).
[16] Y. Seo, G. Song, P. Kim, S. Sachdev, S.-J. Sin, Phys. Rev. Lett. **118**, 036601 (2017).
[17] J. M. Link, B. N. Narozhny, E. I. Kiselev & J. Schmalian, Phys. Rev. Lett. **120**, 196801 (2018).
[18] A.V Andreev, S.A. Kivelson, and B. Spivak, Phys. Rev. Lett. **106**, 256804 (2011).
[19] M. Schütt, P.M. Ostrovsky, I.V. Gornyi, and A.D. Mirlin, Phys. Rev. B **83**, 155441 (2011).
[20] B.N. Narozhny, I.V. Gornyi, M. Titov, M. Schütt, and A.D. Mirlin, Phys. Rev. B **91**, 035414 (2015).
[21] D. E. Sheehy, J. Schmalian, Phys. Rev. Lett. **99**, 226803 (2007).
[22] I. F. Herbut, V. Juricic, O. Vafek, Phys. Rev. Lett. **100**, 046403 (2008).
[23] E. G. Mishchenko, Europhys. Lett. **83**, 17005 (2008).
[24] D. E. Sheehy, J. Schmalian, Phys. Rev. B **80**, 193411 (2009).
[25] A. Golub and B. Horovitz, Phys. Rev. B **81**, 245424 (2010).
[26] V. Juricic, O. Vafek, I.F. Herbut, Phys. Rev. B **82**, 235402 (2010).
[27] S. H. Abedinpour, G. Vignale, A. Principi, M. Polini, W.-K. Tse, and A. MacDonald, Phys. Rev. B **84**, 045429 (2011).
[28] I. Sodemann and M. M. Fogler, Phys. Rev. B **86**, 115408 (2012).
[29] B. Rosenstein, M. Lewkowicz and T. Maniv, Phys. Rev. Lett. **110**, 066602 (2013).
[30] G. Gazzola, A. L. Cherchiglia, L. A. Cabral, M. C. Nemes and M. Sampaio, Europhysics Letters **104**, 27002 (2013).
[31] S. Teber and A. V. Kotikov, Europhysics Letters **107**, 57001 (2014).
[32] J. M. Link, P. P. Orth, D. E. Sheehy, and J. Schmalian Phys. Rev. B **93**, 235447 (2016).
[33] R. R. Nair, P. Blake, A. N. Grigorenko, K. S. Novoselov, T. J. Booth, T. Stauber, N. M. R. Peres, A. K. Geim, Science **320**, 1308 (2008).
[34] T. Stauber, N. M. R. Peres, and A. K. Geim, Phys. Rev.

B **78**, 085432 (2008).
[35] S. Conti and G. Vignale Phys. Rev. B **60**, 7966 (1999).
[36] E. I. Kiselev and J. Schmalian, preprint arXiv:1806.03933 (2018).
[37] D. Forcella, J. Zaanen, D. Valentinis, and D. van der Marel, Physical Review B **90**, 035143 (2014).
[38] B. Bradlyn, M. Goldstein, and N. Read, Phys. Rev. B **86**, 245309 (2012).
[39] A. Principi, G. Vignale, M. Carrega, and M. Polini, Phys. Rev. B **93**, 125410 (2016).
[40] V.B. Berestetskii, E.M. Lifshitz, and L.P. Pitaevskii, *Quantum Electrodynamics* (Pergamon Press, 1980).
[41] M. Mecklenburg and B. C. Regan, Phys. Rev. Lett. **106**, 116803 (2011); Erratum Phys. Rev. Lett. **106**, 229901 (2011).
[42] L.D. Landau and E.M. Lifshitz, *The classical theory of fields* (Pergamon Press, 1975).
[43] C. Itzykson and J. Zuber, *Quantum Field Theory* (McGraw-Hill, 1988).
[44] F. J. Belinfante, Physica **7**, 449 (1940).
[45] L. Rosenfeld, Acad. Roy. Belg. Memoirs de classes de Science **18** (1940).
[46] R. Kubo, Journ. of the Phys. Soc. Jpn. **12**. 570 (1957).
[47] G.D. Mahan, *Many Particle Physics*, Plenum, New York, 1990.
[48] J.M. Luttinger, Phys. Rev. **135**, A1505 (1964).
[49] G. A. Inkof, J. Küppers, J. Link, B. Goutéraux, and J. Schmalian, preprint.
[50] P. C. Martin and J. Schwinger, Phys. Rev. **115**, 1342 (1959).
[51] D. C. Elias, R. V. Gorbachev, A. S. Mayorov, S. V. Morozov, A. A. Zhukov, P. Blake, L. A. Ponomarenko, I. V. Grigorieva, K. S. Novoselov, F. Guinea, and A. K. Geim, Nature Physics **7**, 701 (2011).